ACS Sustainable Chemistry & Engineering

pubs.acs.org/journal/ascecg

Perspective

Sustainable Production of Layered Bismuth Oxyhalides for Photocatalytic H_2 Production

Matthew N. Gordon, Kaustav Chatterjee, Nayana Christudas Beena, and Sara E. Skrabalak*

Cite This: *ACS Sustainable Chem. Eng.* 2022, 10, 15622−15641

Read Online

ACCESS | Metrics & More | Article Recommendations

ABSTRACT: Bismuth oxyhalides ($Bi_aO_bX_c$ X = Cl, Br, I) are promising layered photocatalysts that can produce H_2 using solar light. The layered crystal structures minimize electron−hole recombinations in these materials and provide compositional flexibilities that allow for band gap tuning. Current literature highlights developments in synthetic routes and improved performance metrics; however, an analysis of the sustainability of these compounds is missing. In this Perspective, we use the life cycle assessment framework as a guide to evaluate the sustainability of each stage of the bismuth oxyhalide life cycle, from raw material extraction (mining, refinement, purification) all the way through the end of the material's life and consider ways to recycle and/or reuse the spent photocatalyst. Here, we gather and unite information from the bismuth oxyhalide field with information from the sustainability literature in the first attempt to evaluate the sustainabilities of these materials as photocatalysts for H_2 production. We present our own perspective on the future of the field and make recommendations for researchers interested in this class of materials and photocatalysts more broadly.

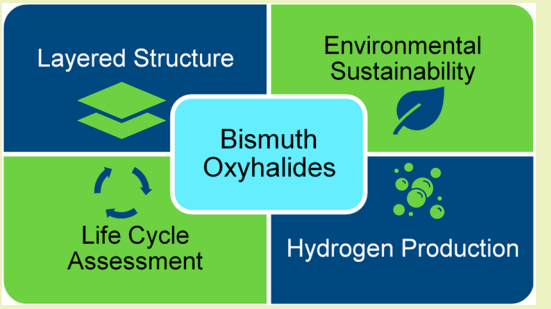

KEYWORDS: *bismuth oxyhalides, life cycle assessment, layered nanomaterials, hydrogen production, sustainability*

INTRODUCTION

Overview. Bismuth oxyhalides are valuable photocatalytic materials for solar H_2 production. Through this Perspective, we discuss these materials with a focus on their sustainability from cradle to grave. With life cycle assessment (LCA) methodology, we discuss the environmental impacts of each phase of bismuth oxyhalide's journey: from raw material extraction to the synthesis and use of bismuth oxyhalides, and finally, the end of the material's life cycle (Figure 1). Our discussion reveals gaps in knowledge that limit a full LCA but also facilitate a broader critique of photocatalytic material selection. For example, our literature survey revealed that many articles detail new synthetic methods or improved metrics of material performance without commentary of the environmental impact of the promoted materials. Understandably, lab-scale efficiency studies are not scalable to global markets, which will be required of future photocatalyst systems, but material sustainability must be a part of the conversation from the start, given that the overarching goal is to use these materials for sustainable fuel generation. Thus, this Perspective integrates current bismuth oxyhalide research with sustainability metrics to begin evaluation of this material class as a potential solution to the energy crisis.

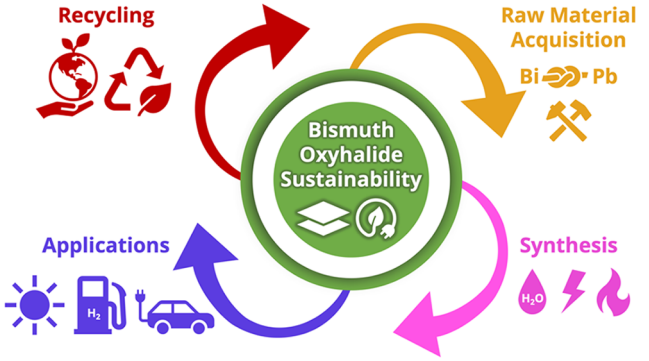

Figure 1. Pictorial representation of the sustainability of the bismuth oxyhalide life cycle.

H_2 Economy. Hydrogen (as H_2) offers a promising alternative to fossil fuels. H_2 has high energy content per unit mass (142.0 MJ/kg),[1] is lightweight, is storable for long periods of time, and can be produced on a global scale making it preferrable to electric batteries for many energy storage applications.[2] A "hydrogen economy" has been envisioned

Received: September 5, 2022
Revised: November 3, 2022
Published: November 21, 2022

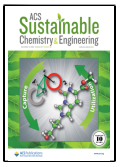

with reduced fossil fuel dependence across all sectors and is steadily becoming reality.[3−10]

However, fossil fuels are used to produce nearly all the world's H_2, with 6% of natural gas and 2% of coal going directly to the production of H_2. Such production results in 830 megatons of CO_2 emissions per year (comparable to the combined CO_2 emissions of Indonesia and the United Kingdom).[2] Thus, considerable research is underway to produce "green" H_2 without carbonaceous byproducts using renewable energy sources like solar and wind. The expansion of H_2 as an energy carrier additionally benefits the continued development of the global renewable energy infrastructure by providing a long-term storage solution for solar and wind generated energy, whose intermittent production does not always match energy demand.[11] Further, H_2 can be transported worldwide from regions with abundant renewable energy sources to regions where solar and wind resources are not economical.[12]

LCAs of a H_2 economy have been conducted and provide excellent guidance toward the possibilities and limitations of H_2 production and utilization.[13−16] This analysis goes beyond the scope of our Perspective, and we refer readers to the cited publications. A detailed analysis of the efficiency of the packaging, distribution, storage, and transfer of H_2 was conducted by Bossel et al.[1] Here, we discuss photocatalysts designed to produce H_2 from solar water splitting, focusing first on their broad operating principles then specifically the interest in bismuth oxyhalides as a promising class of photocatalysts.

Solar-to-Hydrogen. Solar-to-hydrogen energy conversion offers an incredibly advantageous method of storing sustainable energy via water splitting. As water is an abundant resource on our planet, water splitting provides a platform for sustainable H_2 production. This renewable energy technology has the potential to be scaled up to a commercial plant for H_2 generation and consumption. But, to realize this technology, there are challenges associated with achieving efficient, cost-effective water splitting on a global scale.[10] One particular advantage of using particulate photocatalysts (heterogeneous catalysis) in photocatalytic water splitting is the ease of separation of the catalyst dispersion mixture after catalysis, making it viable for commercialization compared to homogeneous counterparts.[10,17] Further, powder suspensions of particulate photocatalysts provide an inexpensive approach compared to thin film fabrication of heterogeneous photocatalysts by lowering the special fabrication costs of uniform deposition of films.

Three crucial steps for photocatalytic water splitting reactions with heterogeneous photocatalysts are (i) photon absorption, (ii) separation and transportation of charge carriers, and (iii) facilitation of the reduction and oxidation half reactions. The efficiencies of these steps are dependent on the intrinsic properties of the semiconductor photocatalyst, such as its band gap, energies of conduction and valence bands, and charge carrier effective masses. The overall water splitting reaction and component half reactions are summarized in eqs 1−5 (h^+ and e^- denotes photogenerated holes and electrons, respectively):

Overall water splitting:

$$2H_2O_{(l)} \rightarrow 2H_{2(g)} + O_{2(g)} \quad (1)$$

Hydrogen evolution reaction (HER):

$$\text{acidic: } 2H^+ + 2e^- \rightarrow H_{2(g)} \quad (2)$$

$$\text{alkaline: } 2H_2O_{(l)} + 2e^- \rightarrow H_{2(g)} + 2OH^- \quad (3)$$

Oxygen evolution reaction (OER):

$$\text{acidic: } 2H_2O_{(l)} + 4h^+ \rightarrow O_{2(g)} + 4H^+ \quad (4)$$

$$\text{alkaline: } 4OH^- + 4h^+ \rightarrow O_{2(g)} + 2H_2O_{(l)} \quad (5)$$

The rate of gas evolution (H_2 and O_2) is specified with a standard unit, e.g., μmol h^{-1} g^{-1}, and the photocatalytic activity differs based on the experimental conditions such as irradiation light source, type of catalysis reactor, and electrolyte. Due to these differences, the photocatalytic activities of photocatalysts are often difficult to be directly compared with each other. To mitigate this challenge, determination of quantum yield is a viable and accepted solution by comparing the amount of product (reacted electrons) and the incident number of photons. The photon flux can be measured using a photodiode or power meter, although we note that determination of the exact number of photons absorbed by a photocatalyst in a dispersed system is difficult owing to scattering of light by particles. So, the obtained quantum yield is an apparent quantum yield (AQY). The AQY is defined as the ratio

$$\text{AQY}\,(\%) = \frac{\text{Number of reacted electrons}}{\text{Number of incident photons}} \times 100 \quad (6)$$

Further, to obtain a direct correlation between solar energy absorbed to H_2 output in a large-scale panel-based reactor, solar-to-hydrogen (STH) conversion efficiency can be used. STH is defined by the ratio

$$\text{STH}\,(\%) = \frac{\text{Output energy as } H_2}{\text{Energy of incident solar light}} = \frac{H_2 \text{ rate (mmol } s^{-1}) \times (237.2\,\text{kJ mol}^{-1})}{(100\,\text{mW cm}^{-2}) \times \text{Irradiaiton area (cm}^2)} \quad (7)$$

Photocatalysts. Photocatalytic materials used in water splitting are composed mainly of d^0 or d^{10} metal oxides, sulfides, nitrides, etc., with recent emphasis moving toward metal heteroanionic materials such metal oxyhalides, oxysulfides, oxynitrides, etc.[17−19] Photocatalysts with layered crystal structures have also gained significant attention, including metal-containing and metal-free materials.[20,21] The electrostatic stacking of oppositely charged layers makes layered materials exciting due to in-plane charge carrier delocalization.[18] Of this class of materials, we focus our Perspective on layered bismuth oxyhalides.

BISMUTH OXYHALIDES ($Bi_aO_bX_c$)

Bismuth oxyhalides $Bi_aO_bX_c$ (X = Cl, Br, and I) are promising layered materials for solar energy harvesting owing to their unique crystal structures and suitable electronic structures. Bismuth oxyhalides are V−VI−VII ternary compound semiconductors that have layered crystal structures with alternating charged layers of $[Bi_aO_b]^{z+}$ and z number of X^- layers. Their strong intralayer covalent bonding coupled with weak interlayer van der Waals interactions lead to greater anisotropic structural, optical, electrical, and mechanical properties.[20,22]

Research has been dedicated to the development of bismuth oxyhalide nanostructures with well-defined structural features to improve their photocatalytic performances. However, less research has been dedicated to the fundamental role of the unique layered structures on their photocatalytic activities. The unique layered structures of BiOX nanomaterials offer many

https://doi.org/10.1021/acssuschemeng.2c05326
ACS Sustainable Chem. Eng. 2022, 10, 15622−15641

advantages. One advantage is that the pH value of the surrounding environment affects the layered structure.[20] Changing the pH of the nanocrystal solution works as a synthetic lever to access other $Bi_aO_bX_c$ stoichiometries, generating new layered semiconductors. The crystal structures of these materials (Figure 2) are layered, with different compositions of the individual layers leading to different band gaps and band structures, which may be favorable in terms of light absorbance capability, charge carrier transfer, and band positions.

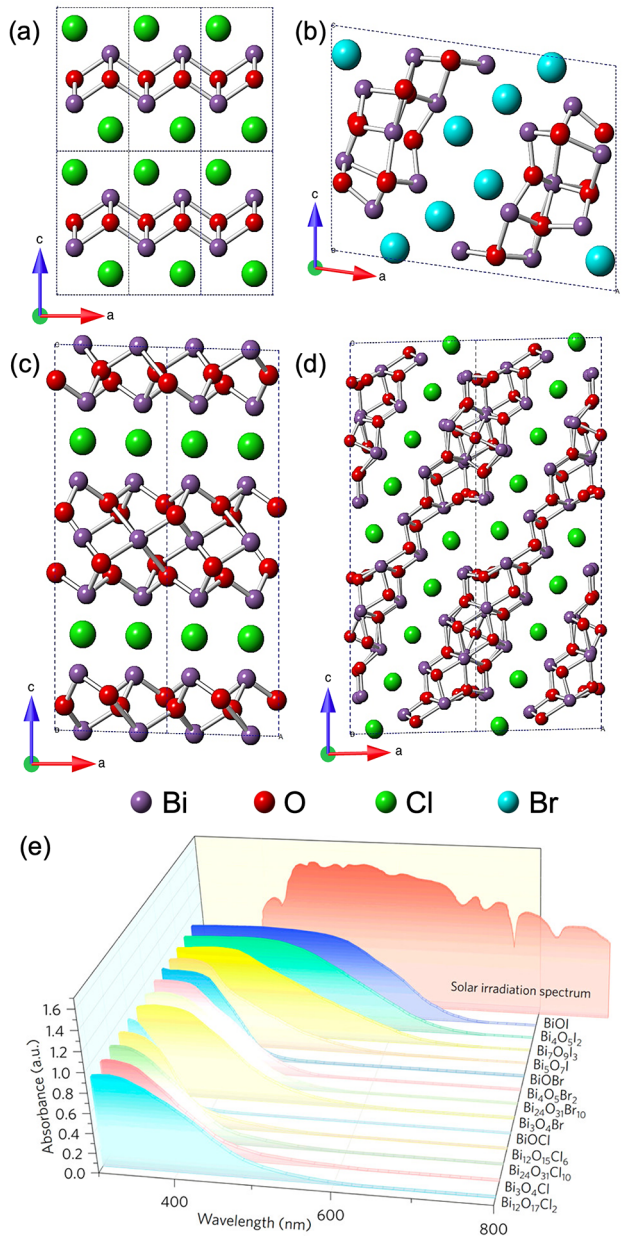

Figure 2. Crystal structures of different bismuth oxyhalides: (a) BiOCl, (b) $Bi_4O_5Br_2$, (c) Bi_3O_4Cl, and (d) $Bi_{24}O_{31}Cl_{10}$ as examples. Images generated from CIFs from refs 23−26 with permission. Copyright 2014, American Chemical Society; Copyright 2001, Walter de Gruyter and Company; Copyright 1998, Walter de Gruyter and Company; Copyright 2000, International Union of Crystallography. (e) Optical absorption spectra of $Bi_aO_bX_c$ materials. Reproduced with permission from ref 27. Copyright 2017, American Chemical Society.

Facet-selective growth of these layered structures can optimize the resulting surface exposure to facilitate water splitting.[28] That is, the interactions of adsorbed protons and water with photogenerated electrons and holes, respectively, can be tuned through selective surface expression, which allow for selective manipulation of the activation processes.[20] Another advantage of the layered crystal structure is that alternating positive and negatively charged layers in the crystal structures form static internal electric fields along the *c*-axis (perpendicular to the charged layers). Photoinduced separations and transfers of charge carriers from the bulk to the surface are promoted by the internal electric fields generated by the characteristic layered structures, which are advantageous to the ensuing surface photocatalytic reactions. In addition, facile charge transportation and enhanced separation efficiencies of the photoinduced electron−hole pairs have also been achieved by inducing oxygen vacancies in the crystal structures of bismuth oxyhalides.[29]

The rate-determining step for water splitting is the oxidation of water to produce O_2. The reduction process involves two electrons combining with $2H^+$ to form H_2. O_2 production, however, is kinetically sluggish as four holes are required to oxidize H_2O to produce O_2. Thus, improvement of the water splitting oxidation half-reaction is necessary for the improved efficiency of H_2 generation. Previous studies report O_2 production from BiOX materials with different halogens.[20,30] The valence band maximum (VBM) of BiOX changes as the halide identity changes from Cl to Br to I.[31] The upward shift of VB from Cl to I along with the conduction band minimum (CBM) remains mostly unchanged, allowing for band gap tuning. Likewise, $Bi_aO_bX_c$ materials can produce O_2 photocatalytically, owing to variable VB edges and tunable photoabsorption capabilities by tailoring the stoichiometry.[32]

Photocatalytic H_2 evolution is a promising platform to convert unlimited solar energy to H_2. Results show that $Bi_aO_bX_c$ is photocatalytically active for evolution of H_2.[20] The possibility of band structure tailoring of $Bi_aO_bX_c$ owing to the compositional changes possible by varying atomic ratios of Bi, O, and X enables efficient HER. The CB can be modulated by the variation of Bi content and the VB can be modulated by the variation of O and halide contents.[32] Further, by engineering surface oxygen vacancies, heterojunction formation, cocatalyst loading, or doping into bismuth oxyhalides, enhanced H_2 production has been reported.[33]

INTRODUCTION TO LIFE CYCLE ASSESSMENTS

With understanding of the potential of bismuth oxyhalides as photocatalysts, we now look at the environmental impact of these materials.

LCA is a systematic evaluation of the environmental inputs and outputs of a production process through time, including all the actions to make, transport, use, and dispose of a product (also known as "cradle to grave") (Figure 3a).[34] LCAs address the need for consumers, industry, and governmental bodies to monitor and protect the environment and minimize pollution and waste. Further, LCAs can be used to compare product and system costs and efficiencies. Simply, a LCA uses scientific data to support decision making.

Early studies on the environmental impacts of products and materials emerged in the 1960s and 1970s with broad areas of focus. The need for the assessment across all life stages of a product stems from the fact that a large part of the total ecological impact of a product is not simply in the *use* of a

https://doi.org/10.1021/acssuschemeng.2c05326
ACS Sustainable Chem. Eng. 2022, 10, 15622−15641

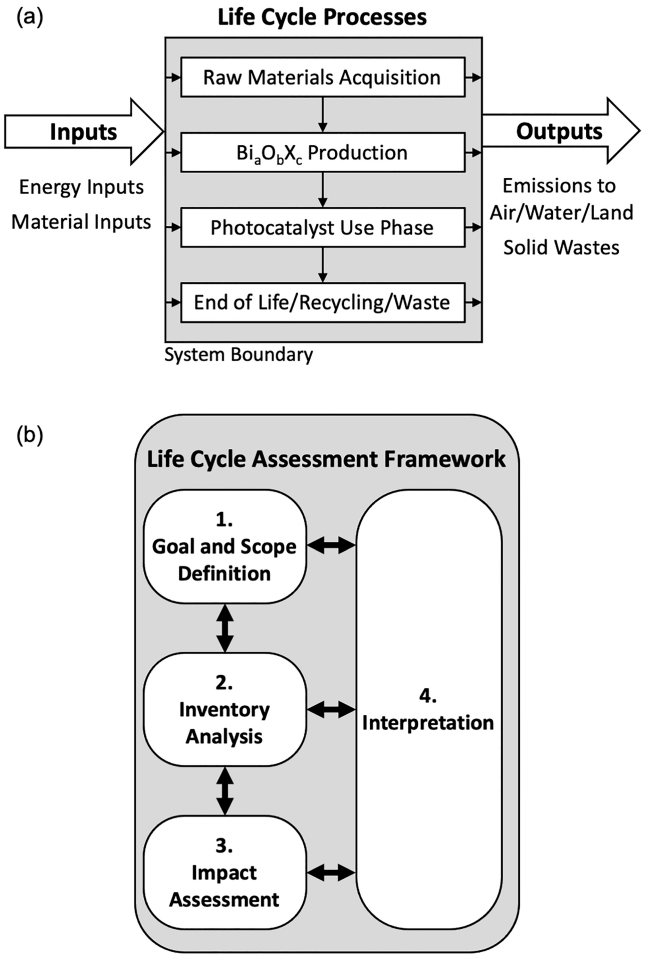

Figure 3. (a) Main stages and typical inflows and outflows in a LCA. Adapted from ref 35. (b) Phases of a LCA. Adapted with permission from ref 36. Copyright 2006, International Organization for Standardization.

product, but rather in its raw material extraction, production, transportation, and ultimate disposal. LCA standardization came in the 1990s and early 2000s with the publication of International Organization for Standardization (ISO) 14040 and ISO 14044, which now outline the framework and guidelines for LCAs.[36,37] We note here that our analysis of bismuth oxyhalides is modeled after these international standards but is not a formal LCA as differences are present. We place emphasis on where more data are needed to fully evaluate these promising materials. Additionally, LCA does not represent a comprehensive or complete assessment tool. Other factors may be present such as costs, and such factors can change over time. Therefore, subjective judgment is present at various steps.

The LCA model includes four phases that are goal and scope definition, inventory analysis, impact assessment, and interpretation (Figure 3b). The goal of a LCA defines the aim, intended audience, and application of the study, while the scope of a LCA defines the system boundaries, functional unit, data assumptions, and limitations. The inventory analysis phase contains the data collection and quantifies all relevant inputs and outputs of the system. The impact assessment phase weighs the magnitude of the environmental effects from the data collected in the inventory analysis. The interpretation phase analyzes the data of the individual impact assessments in the combined context of the entire life cycle. It further makes conclusions and recommendations consistent with the data and discusses limitations of the LCA. These four phases of the LCA model are ultimately not linear, and a final LCA is achieved through a very iterative process as shown in Figure 3b. As data are obtained and evaluated, the goal and scope may change. New data may need to be collected and reviewed, and conclusions may change. Thus, it is important to be flexible in each phase to ultimately deliver a LCA that is consistent and complete.

Having outlined the LCA and its phases, we now introduce our study into the LCA of layered bismuth oxyhalides. Acknowledging the need for novel and sustainable energy production, photocatalysis has been promoted as a solution to generate solar fuels (e.g., H_2). By combining sunlight and a proton source (such as water) in the presence of an appropriate photocatalyst, H_2 can be readily formed. In the literature, photocatalysts are commonly evaluated by their quantum efficiencies, a metric that captures the effectiveness of light absorption and energy conversion to usable form. This oversimplification, however, neglects many other steps of a photocatalyst's life cycle beyond the use phase. Further, it measures only performance and does not capture the sustainability of the methods used. A more holistic analysis would look deeper at the photocatalyst at all stages, from raw material extraction and photocatalyst synthesis to use and end of life disposal and the sustainability of each of these stages. If photocatalysis is to be the solution to the looming energy crisis, then photocatalysts must be able to be produced efficiently on a global scale with minimal harmful waste streams, robust recycling systems, etc.

Here, we create a qualitative LCA of layered bismuth oxyhalides to support a deeper understanding of the sustainability of a known potential photocatalyst and for later comparisons to other materials. While the precise environmental effect of any single step may not be quantitatively known, we aim to find areas that need further optimization or limit the overall use of bismuth oxyhalides in a qualitative sense. At the end of the LCA, we conclude and make recommendations as to the future of the field and the utility of bismuth oxyhalide materials as photocatalysts.

This LCA is focused on bismuth oxyhalides for solar *photo*catalysis only. Bismuth oxyhalides are less useful as electrocatalysts, so these applications are not considered.[38] We further focus on water splitting as a route to produce H_2. Other proton sources such as formic acid are not considered. We define bismuth oxyhalides as the class of compounds of the type $Bi_aO_bX_c$ (where X = Cl, Br, I). Such compositions include BiOCl, BiOBr, and BiOI, as well as other stoichiometries such as Bi_3O_4X, $Bi_4O_5X_2$*, and $Bi_{24}O_{31}X_{10}$.[23−26] *Note that $Bi_4O_5Cl_2$ is not layered, but $Bi_4O_5Br_2$ and $Bi_4O_5I_2$ are layered.[24,39,40]

Defining the functional unit of this study is challenging. Metrics such as per mole or kg of H_2 produced are not possible, as each compound has different performances, and these additionally differ based on the synthesis method and factors like cocatalyst loading. A simple weight unit such as per kg photocatalyst could be used. However, there are multiple formulas, so the composition varies between materials. Thus, a functional unit of energy/resources/cost/etc. to produce 1 kg BiOCl is used as an initial framework. As we explore other materials with other halogens and stoichiometries, these materials can be evaluated and "converted" to this functional unit.

https://doi.org/10.1021/acssuschemeng.2c05326
ACS Sustainable Chem. Eng. 2022, 10, 15622−15641

Our system boundary represents a "cradle to grave" analysis: the acquisition of raw materials, manufacturing inputs and outputs, photocatalyst synthesis techniques with inputs and outputs (including the use/production of fuels, electricity, and heat), photocatalyst use period, and ending with spent photocatalyst reuse/repurposing/recycling/disposal (Figure 3a). We note that certain components of this analysis are much more developed than others based on available information. Moving into the second and third phase of a LCA, inventory analysis and impact assessment, we look at each stage of the life cycle individually to assess the relevant inputs and outputs of each section and evaluate the sustainability of each process step.

This Perspective concludes with the fourth phase of a LCA, the interpretation phase. The strengths and weaknesses in the sustainability of each life cycle step are assessed with respect to the entire life cycle. We make conclusions and recommendations on the future of bismuth oxyhalide production and the sustainability that must be researched further before this material can be used as a solution to the global energy crisis. More broadly, we outline areas where more information is needed and place this information within the field of photocatalysis.

RAW MATERIALS

Bismuth-based nanomaterials have been gaining interest as promising photocatalysts as outlined in the Introduction and Bismuth Oxyhalides ($Bi_aO_bX_c$) sections. Bismuth has been known since antiquity and was often mistaken as lead and tin. Bismuth is found naturally as the native metal and in ores such as bismuthinite (Bi_2S_3) and bismite (Bi_2O_3); however, due to the rare occurrence of bismuth minerals in sufficient quantities to be mined as the principal products, bismuth is mainly obtained commercially as a byproduct from refining ores of different metals, mainly lead, but also copper and tin.[41−44] Bismuth has a crustal abundance of 0.1−0.2 ppm, making it the least abundant element in the nitrogen group.[45] In the USA manufacturing sector for 2016, bismuth possessed a mineral commodity supply risk (SR) of 0.5 on a scale from 0 (very low risk) to 1 (very high risk).[46] SR is calculated as the geometric mean of three key indicators: disruption potential, trade exposure, and economic vulnerability. For comparison, lithium, selenium, and zirconium have low SR scores (0.2−0.3). Indium, strontium, and tellurium have moderate SRs (0.3−0.4), while bismuth, gallium, iridium, and lanthanum have high SRs (0.5−0.6). Since bismuth is most often produced as a byproduct of processing lead ores, world reserves of bismuth are typically estimated from that contained in lead ores.[44] Historically, bismuth has only been mined as a principal product in two places: the Tasna mine in Bolivia (inactive since 1996) and a mine in China.[44] Annual global production of bismuth in 2021 was 19,000 t, with dominant production coming from Asia (Table 1).[44]

The USA ended production of primary refined bismuth in 1997 and thus relies completely on imported bismuth.[44] The USA maintains no government stockpile, despite being deemed a critical mineral in 2018.[47] Similarly, bismuth was named a critical raw material by the European Commission in 2017.[48] Bismuth is present in some lead ores mined in the USA, but even this source is exported for smelting (the last primary lead smelter in the USA closed in 2013). In 2021, the USA had a net import reliance (as a percentage of apparent consumption) of 90%.[44] This parameter is broken down by country of import in Table 2. The price of bismuth in 2021 in the USA was $8.05 US per kg ($3.65 US per pound). Globally, the average bismuth price from 2007 to 2014 was $17.28 US per kg ($7.84 US per pound).[44]

Table 1. Global Refinery Production of Bismuth in 2021 by Country in Metric Tons and Percent of Total[a]

Country	2021 Refinery Production (metric tons)	2021 Refinery Production (%)
China	16,000	84
Republic of Korea	1000	5
Laos	1000	5
Japan	600	3
Kazakhstan	240	1
Bolivia	60	0.3
Bulgaria	50	0.3
Canada	30	0.2
Mexico	10	0.05
Total	19,000	

[a]Adapted from ref 44.

Table 2. Sources of Bismuth Imported to USA from 2017−2020 by percent[a]

USA Import Sources (2017−2020)	Percentage
China	67
Republic of Korea	16
Mexico	6
Belgium	5
Other	6

[a]Adapted from ref 44.

A total of 90% of the world bismuth production is as a byproduct of lead metallurgy.[49] Because the bismuth life cycle is inherently linked with lead production, to understand the life cycle of bismuth, we must also explore the refinement of lead to produce pure bismuth. The processing and refining route of bismuth-containing ores is based on the bismuth content of the ore and the strategy for recovering the other metals, mainly lead (Figure 4). Several methods of purifying lead ore include electrorefining (Betts process), pyrorefining (Kroll−Betterton process), ionometallurgy, and a combination of gravity, flotation, and magnetic separation.[50] The first two of these methods are the most commonly used, and the sustainability of each is discussed in detail below. The Betts process (18% of all bismuth processed) is preferred when the bismuth content of the lead concentrate is >4%, while the Kroll−Betterton process (61% of all bismuth processed) is preferred for 0.05%−3.5% bismuth.[50,51]

The Betts process for electrorefinement of lead involves using an impure metal alloy as an anode that undergoes electro-oxidation to remove lead, leaving other impurity metals (including Bi) as an undissolved anode slime (~3−10 wt % Bi).[45,52] In this process, lead fluorosilicate ($PbSiF_6$) and hexafluorosilicic acid (H_2SiF_6) are used as the electrolyte. H_2SiF_6 is used due to its low cost; however, it decomposes into hydrofluoric acid and silicon tetrafluoride by the following reaction:

$$H_2SiF_6 \rightarrow 2HF_{(g)} + SiF_{4(g)} \quad (8)$$

Both HF and SiF_4 are corrosive, toxic gases which are environmentally costly. The Betts process uses ~554 MJ per ton lead for the electrolysis process and 166 MJ per ton lead for other mechanical considerations for a total of 720 MJ per ton

https://doi.org/10.1021/acssuschemeng.2c05326
ACS Sustainable Chem. Eng. 2022, 10, 15622−15641

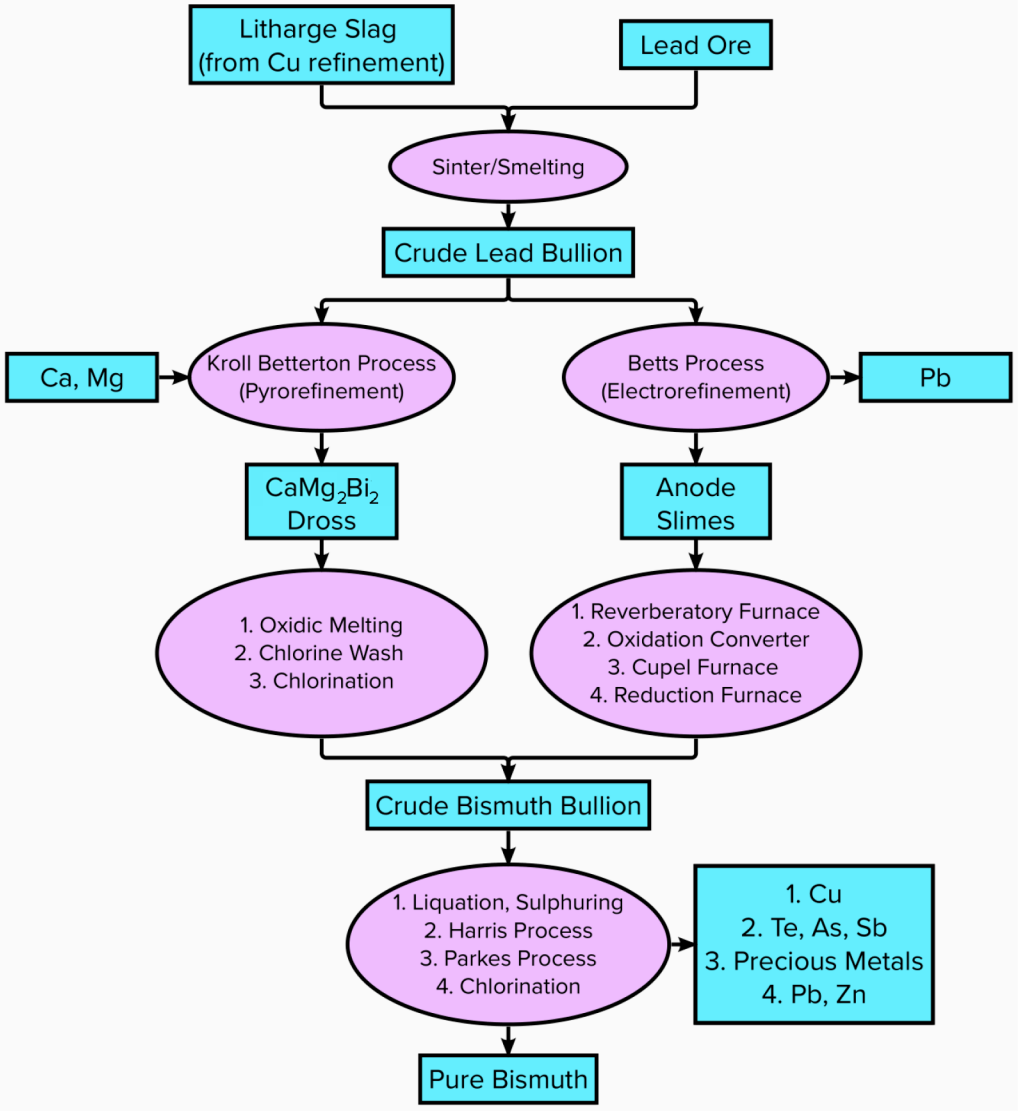

Figure 4. Simplified flowchart of bismuth production. Blue rectangles represent material input and outputs. Purple ovals are process, and numbered processes are sequential. Adapted with permission from refs 45 and51. Copyright 1992, Springer Nature. Copyright 2002, Maarten van den Tweel.

lead (using the data from ref 52 by taking an average of seven lead electrorefining plants weighted by annual lead production).

The Kroll–Betterton process for pyrorefinement of lead involves the addition of magnesium (metallic) and calcium (as a 5% Ca in lead alloy) to the molten impure alloy.[45,53] These metals are stirred at 420 °C and then slowly cooled almost to the lead freezing point of 327 °C. $CaMg_2Bi_2$, an intermetallic compound with a higher melting point and lower density than molten lead, forms as a solid dross on the surface of the molten lead which can be skimmed off. The overall reaction is shown by the equation

$$Ca + 2Mg + 2Bi \rightarrow CaMg_2Bi_{2(s)} \quad (9)$$

which has a solubility product constant in molten lead of $10^{-7.37}$.[54] This process can be performed in both continuous and batch reactions. The resulting material is treated with chlorine to remove the calcium and magnesium, leaving a lead–bismuth alloy that is ~7 wt % bismuth.

The remaining bismuth alloy from either the Betts or Kroll–Betterton processes is further refined to obtain pure bismuth.[45] If the alloy contains excess copper (which remains through the Betts process), sulfur drossing is performed to remove it.[55] Tellurium, tin, arsenic, and antimony can be removed with the Harris process by mixing in molten NaOH and NaCl.[56−58] Other metals are then removed by bubbling in chlorine gas. Once the alloy reaches ~70% bismuth, desilvering takes place using the Parkes process, a liquid–liquid extraction using molten zinc which extracts any precious metals.[51,59,60] Chlorine refining is then continued to achieve >99.99% purity bismuth.

It is clear that bismuth production is interwoven with many other systems, too many to be adequately addressed here. The overall bismuth production process can be evaluated for its sustainability by various metrics. No large database such as Ecoinvent has data on bismuth metal, but others have put together data on materials using or related to bismuth.[61−64] Nuss and Eckelman have tabulated excellent, extensive data on the LCA of metals including bismuth.[62] We present some of their bismuth-specific data in Table 3. Using 2008 data, they summarize the global warming potential (GWP) of bismuth production to be 58.9 kg CO_2-eq/kg bismuth and the cumulative energy demand (CED) to be 697 MJ-eq/kg bismuth (cradle to gate values). Notably, both are broken down by

https://doi.org/10.1021/acssuschemeng.2c05326
ACS Sustainable Chem. Eng. 2022, 10, 15622−15641

Table 3. Environmental Impact of 1 kg of Bismuth Production[a]

Metric	Value	Rank[b]
Global Warming Potential	58.9 kg CO_2-eq/kg Bi	36
Cumulative Energy Demand	697 MJ-eq/kg Bi	34
Terrestrial Acidification Potential	0.38 kg SO_2-eq/kg Bi	34 (Tied)
Freshwater Eutrophication	0.022 kg P-eq/kg Bi	32
Human Toxicity Impact	0.000017 CTUh/kg Bi	23

[a]Adapted from ref 62 which has a Creative Commons Attribution 4.0 International License, published by the Public Library of Science. [b]Of 63 metals studied in ref 62, values correspond to data from 2008 and covering from cradle to gate only (ore mining, concentration, purification, and refining). For all categories, the least harmful is rank 1; the most harmful is rank 63.

process steps and show that 95% of the GWP and 92% of the CED come from the purification/refining processes alone. Mining and concentration steps constitute the rest of the GWP and CED. For context and comparison, the production of steel has a GWP of 2.3 kg CO_2-eq/kg and CED of 23 MJ-eq/kg, whereas cradle-to-gate GWP of Pt, one of the best metal cocatalysts for photocatalytic hydrogen evolution reaction, is 12,500 kg CO_2-eq/kg with a CED value of 243,000 MJ-eq/kg.[62,65,66] Delving deeper into the specific inputs and outputs of bismuth production, Andrae et al. quantified many metrics presented in Table 4.[63]

The other main reagent of $Bi_aO_bX_c$ production is a source of halide ions, mainly halide salts. Ecoinvent v2.0 (2007) has reviewed LCA data for NaCl (Table 5).[67] LCA data for bromide and iodide ions from salts are not tabulated in databases. It can be qualitatively speculated, however, that the environmental impact of bromide and iodide will be more severe due to relative atomic abundancies and the ease in which NaCl can be harvested from ocean water in addition to mineral sources. World production, reserves, and salient statistics of bromine and iodine can be found in ref 44.

Comparing the environmental impact of bismuth and halide raw material production, bismuth is environmentally more costly in most metrics. Its intrinsic association with lead production is a serious concern. As global trends move away from the use of lead for greener bismuth, the coproduction of these two elements may change the metallurgical industry landscape from mainly lead production, with the refinement of impurity bismuth, to one that focuses more on bismuth production/efficiency, etc. This outcome may affect mining sites for bismuth-rich ores or even cause the restarting of mines with bismuth as the primary product. Notably, the extremely low toxicity of numerous bismuth compounds has earned bismuth the status of a "green element" with many LD_{50} values greater (less toxic) than that of table salt.[41] Due to this reason, bismuth-containing compounds and alloys are used for cosmetic, industrial, laboratory, pharmaceutical applications and as environmentally friendly substitutes for lead.[44]

$Bi_aO_bX_c$ MATERIALS PRODUCTION

Originating from raw materials, common bismuth compounds (e.g., Bi, $Bi(NO_3)_3$, $NaBiO_3$, Bi_2O_3, and BiX_3) and halide sources (e.g., NaX, KX, HX, or hexadecyltrimethylammonium halide salts, and ionic liquids) are used as reagents in a variety of synthetic methods toward BiOX materials.[68] These methods include hydrolysis of common salts as well as molecular precursor pathways, being commonly coupled with hydrothermal/solvothermal and templated techniques, among others.[68−70] In this section, an overview of these approaches is provided, giving insights to the key compositional and structural benefits of each, as well as evaluating the sustainability of each production method.

Hydrolysis Methods. One of the simplest methods to synthesize BiOX materials is by hydrolysis of bismuth halides by water or bismuth salts with halide salts in water.[71]

Table 4. Ecoprofile for 1 kg Bismuth Production (units in kg)[a]

Inputs:	
Resources:	
Bismuth	1
Coals, various	3.5
Natural gases, various	0.47
Oils, various	4.3×10^{-6}
Outputs:	
Bismuth	1
Emissions to water:	
As	2.9×10^{-6}
Cd	2.2×10^{-6}
Cr	9.5×10^{-6}
Cu	5.9×10^{-6}
Cyanide	2.8×10^{-6}
Pb	2.8×10^{-5}
Hg	2.0×10^{-7}
Ag	1.2×10^{-7}
Sn	3.7×10^{-7}
Emissions to air:	
Cd	4.3×10^{-6}
CO_2	19.1
Cr	2.4×10^{-6}
Cu	4.9×10^{-6}
Cyanide	2.1×10^{-8}
N_2O	3.7×10^{-4}
Dioxins (measured as 2,3,7,8-tetrachlorodibenzo-*p*-dioxin)	9.3×10^{-13}
Pb	5.2×10^{-5}
Hg	1.3×10^{-6}
Methane	0.025
NO_x	0.047
Particulates, various	0.021
Ag	4.7×10^{-13}
SO_2	0.1
SO_x	9.9×10^{-4}
Sn	1.8×10^{-8}

[a]Adapted with permission from ref 63. Copyright 2008, American Chemical Society.

Table 5. Production data for 1 kg NaCl (units in kg, except where noted)[a]

Inputs		Outputs	
Electricity	0.61 MJ	NaCl	1
Light fuel oil	0.00463	Waste (disposed)	0.03
Diesel	0.0001	Waste water, total	3.82
CaO	0.01388	Water (cooling)	2.69
Na_2CO_3	0.01272		
Water (process)	3.82		
Water (cooling)	2.69		

[a]Adapted with permission from ref 67. Copyright 2007, EcoInvent.

https://doi.org/10.1021/acssuschemeng.2c05326
ACS Sustainable Chem. Eng. 2022, 10, 15622−15641

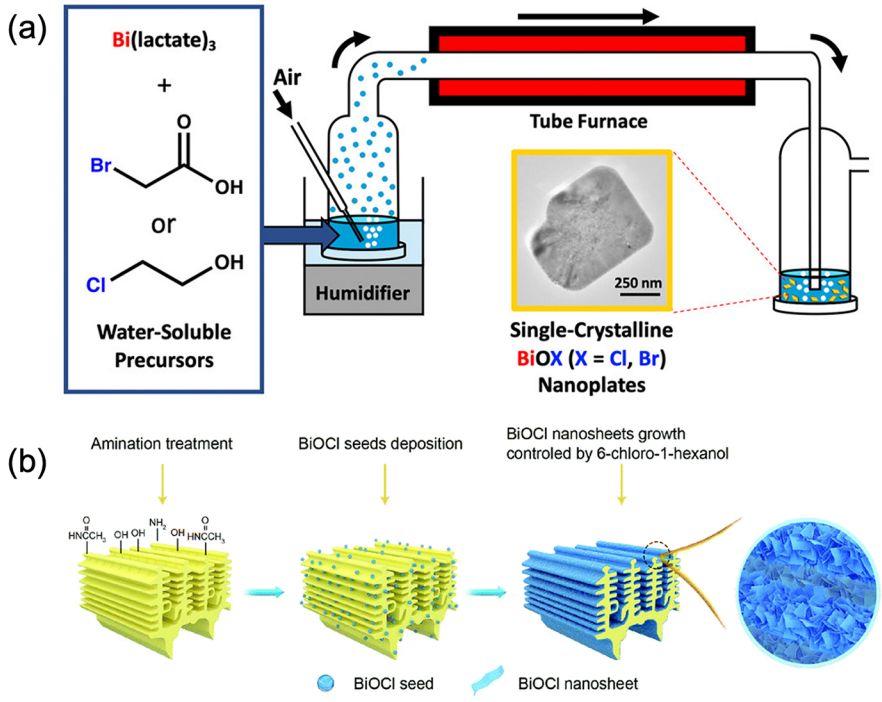

Figure 5. (a) Molecular precursors and schematic of an ultrasonic spray synthesis reactor consisting of a nebulization chamber, hot wall reactor, and collection vessel. A representative transmission electron micrograph of a resulting single-crystalline BiOCl particle is shown. Reproduced with permission from ref 78. Copyright 2020, American Chemical Society. (b) Diagram of the synthesis to produce BiOCl nanosheets on butterfly wing templates. Reproduced with permission from ref 79. Copyright 2017, Royal Society of Chemistry.

Representative reactions are presented as eqs 10 and 11. Often, such syntheses use mild conditions and would be easily scalable, but the BiOX products are powders composed of particles with nonuniform morphology. This outcome arises because of an extremely fast rate of BiOX formation and would limit the ability to leverage particle size, shape, and faceting effects in photocatalysis.

$$BiCl_3 + H_2O_{(l)} \rightarrow BiOCl_{(s)} + 2HCl \quad (10)$$

$$Bi(NO_3)_3 + NaCl + H_2O_{(l)} \rightarrow BiOCl_{(s)} + NaNO_3 + 2HNO_3 \quad (11)$$

Still, there are examples of BiOX materials produced through modified hydrolysis methods that give rise to reasonably defined microscale or nanoscale structures. For example, BiOCl nanoflakes were synthesized by controlled hydrolysis of $BiCl_3$ in the presence of acetylacetone (6 h at 65 °C).[72] In this case, acetylacetone was used as a strongly coordinating solvent to coordinate with BiOCl, and the acidity of the solution was controlled to yield bismuth oxychloride nanostructures from the liquid phase. As a second example, BiOCl nanosheets were produced by hydrolysis of $Bi(NO_3)_3$ in the presence of HCl and Na_2CO_3.[73] In this case, $Bi(NO_3)_3$ and HCl were used as precursors. Bismuth nitrate was dissolved in HCl to produce free Bi^{3+} and Cl^- ions with the pH adjusted to 2 using Na_2CO_3 which led to a slow growth rate of BiOCl to achieve nanosheets.

The selections of commodity salts as reagents and water as a reaction solvent make hydrolysis a green and sustainable approach to produce bismuth oxyhalide photocatalysts. Moreover, the low temperatures of these reactions and the ability to create crystalline materials directly are attractive. However, the reliance on additives to control hydrolysis rates and achieve structurally defined materials can limit the sustainability of such syntheses.

Hydrothermal/Solvothermal Methods. The hydrolysis chemistry outlined in the previous section is often integrated into hydrothermal and solvothermal approaches. In these approaches, a closed vessel is heated to create a high pressure environment, which increases the solubility of precursors and, in turn, their reactivities. This approach also makes use of organic solvents more feasible as common reagents become more soluble at higher pressure. This approach also is particularly attractive to the preparation of BiOX materials in water as the rapid hydrolysis conditions, even at atmospheric pressure, limit control over nucleation and growth processes. However, at high pressure, initial precipitates can be dissolved. This condition yields greater control over the subsequent nucleation and growth processes such that BiOX powders can be produced with control of crystal size, shape, faceting, and stoichiometry. In hydrothermal syntheses, $Bi(NO_3)_3{\cdot}5H_2O$ is widely used as the bismuth source. During the formation process, Bi^{3+} cations hydrolyze with H_2O to yield $BiONO_{3\ (s)}$ and H^+. The formed $BiONO_{3\ (s)}$ reacts with halides to yield BiOX.

Like conventional colloidal syntheses, this synthetic control over composition and structure is achieved by modulating the thermodynamics and kinetics of the intermediates of BiOX formation. For example, Zhang and co-workers reported two-dimensional (2D) structures of BiOCl where the expressed facets were determined by the pH of the hydrothermal synthesis.[74] Notably, low pH conditions gave rise to crystals dominated by {001} facets, while a pH of 6.0 gave rise to crystals dominated by {010} facets. The {001}-terminated BiOCl crystals exhibited greater photocatalytic activity than the {010}-terminated BiOCl crystals for pollutant degradation under ultraviolet (UV) irradiation due to direct semiconductor

https://doi.org/10.1021/acssuschemeng.2c05326
ACS Sustainable Chem. Eng. 2022, 10, 15622−15641

photoexcitation. In contrast, the {010}-terminated BiOCl crystals exhibited greater activity for pollutant degradation with visible light irradiation caused by indirect dye photosensitization.

Facet engineering of BiOX photocatalysts also has been obtained by adjusting the hydrothermal temperature and heating time with different additives. For example, nanoplates with {001} facets exposed on the top and bottom and {110} facets on the sides were achieved by addition of NaCl to $Bi(NO_3)_3$ in a mannitol aqueous solution and autoclaved at 160 °C for 3 h.[75] BiOCl nanospheres were achieved by heating $Bi(NO_3)_3$ in ethylene glycol with KCl as a halide source for 12 h at 160 °C.[76] Here, the Bi^{3+} cations coordinate with ethylene glycol to yield alkoxide complexes and H^+. The {001} surface is capped by H^+ due to the strong binding interaction between the proton and oxygen leading to constrained crystal growth along the *c*-axis leading to {001} facet exposure in the crystals.

Although hydrothermal and solvothermal methods can yield high-quality BiOX nanocrystals, the biggest drawbacks of these synthetic techniques are the high energy cost of heating and the cost of infrastructure needed to generate a high pressure environment. For a more sustainable approach, continuous-flow hydrothermal synthesis with organic solvent minimization (ideally using water instead) needs to be adopted. Further, cost of input and energy consumption are high for these techniques.

Molecular Precursors. Given the difficulty in controlling nucleation and growth of BiOX materials during the hydrolysis of simple salts, researchers have turned to designing molecular precursors. BiOCl nanosheets were obtained by hydrolysis of $Bi_n(Tu)_xCl_{3n}$ (Tu = thiourea).[77] Adjustment of the $BiCl_3$:Tu feed ratio was shown to correlate with the percentage of {001} facet exposure. The photocatalytic activity of the resultant BiOCl was found to be proportional to the percentage of {001} exposure on the particle surface. Recently, our group demonstrated rapid and scalable ultrasonic spray synthesis of BiOX (X = Cl, Br) using molecular precursors (Figure 5a).[78] We identified a bismuth lactate complex and organohalide molecules as water-soluble bismuth and halide sources, respectively. By spatially and temporally confining the precursors in the aerosol phase with molten salt fluxes, these precursors yielded single-crystalline BiOX nanoplates produced in a continuous flow upon heating. Mechanistically, the organohalide molecules react with water at elevated temperatures, releasing the halogen as X^- which immediately reacts with Bi^{3+} to precipitate as BiOX.

The molecular precursor method is also an interesting strategy to produce $Bi_aO_bX_c$ phases. Due to the easy phase transformation with very small pH changes, obtaining high-purity, single-phase $Bi_aO_bX_c$ stoichiometries are challenging when a ≠ b ≠ c. $Bi_4O_5X_2$ (X = Br, I) was obtained by Ye et al. using single-source precursors.[80] In this synthesis, the molecular bismuth, halide, and glycerol precursors were synthesized by a solvothermal process to form the complex precursor. $Bi_4O_5X_2$ was then obtained *via* the hydrolysis of the complex precursor. Two different morphologies were achieved by the authors *via* this method, $Bi_4O_5Br_2$ microspheres and $Bi_4O_5Br_2$ nanosheets. Hierarchical $Bi_4O_5Br_cI_{2-c}$ was also obtained by this molecular precursor method.

To achieve environmental sustainability with molecular precursor methods, further development is still needed, particularly by replacing organic complexes and solvents by water-soluble precursors as we demonstrated. Current methodologies to obtain high quality nanostructures of bismuth oxyhalides using single-source precursors still require high input energy costs such as high temperature and pressure conditions. Continuous-flow reactors such as ours will also add to the sustainability and scalability of these methods. Further, cost of input and energy consumption could be reduced in this type of synthesis technique *via* atom economical routes.

Templated Methods. Bismuth oxyhalides have also been produced by hard and soft templated methods. These methods provide a preformed template on which nucleation can occur through the previously described chemical pathways, lowering the energy barrier to nucleation. Hard templates are solid state materials with defined structures and stable morphologies, such as silica, whereas soft templates have a less defined structure and are able to undergo deformation, such as polymers. The sizes and shapes of the resultant bismuth oxyhalide crystals depend on the type of template used, making it a capable technique for oxyhalide nanostructure synthesis.

Yu and co-workers used a hard template of carbonaceous microspheres and calcined $Bi(NO_3)_3$ and HCl at 400 °C to synthesize hollow microspheres of BiOCl with shell thicknesses of 40 nm.[81] The carbonaceous spheres were coated by adsorbed Bi^{3+} cations because of the many functional groups (−OH and −COOH) on the carbon material as well as halide ions. This adsorption process was followed by calcination. During heating, the carbonaceous spheres contracted and combusted, leading to hollow BiOCl seeds that nucleated and grew and volatilized any excess halogen ions.

Zhang and co-workers demonstrated hierarchical BiOCl by employing butterfly wing scales as soft biotemplates (Figure 5b).[79] The scales had 3D hierarchical photonic structures. They showed that the BiOCl nanosheets can evenly grow on the templated surface and imitate the fine structural features of the butterfly scales through an amination treatment followed by an electroless deposition procedure. They used 6-chloro-1-hexanol as the chloride precursor to achieve uniform replication, with aqueous ethanol as the solvent to reduce the rate of Cl^- release.

Templated methods excel at producing BiOX nanocrystals with well-defined morphologies; however, the production rate and overall yields are low. Continuous-flow templated synthesis with solvent minimization/recycling could be a potential solution, with reducing the cost of the template and energy consumption needed for this type of synthesis technique. Also, the judicious use of biowaste-derived or recyclable templates is another strategy to cut the production cost to yield high quality BiOX nanocrystals for energy harvesting and environmental remediation applications.

Comparative Sustainability of Synthesis Methods. To compare the sustainability of the various synthetic methods and techniques, we look at the process steps that make up each method. Hydrolysis syntheses are the most sustainable with simple reagents, water as the solvent, and little to no heat applied. As a trade-off, the resulting products often lack structural control, which can impact the performance and thus sustainabilities of BiOX materials in the use stage. Hydrothermal methods similarly use simple reagents and water in their processes; however, the application of high temperature heating makes this step less sustainable assuming conventional means of energy input. For solvothermal methods, the energy associated with heating remains similar to hydrothermal methods, but now, the sustainability of the solvent system must be considered, which is anticipated to be less than water. Molecular precursor methods and templated methods are harder to directly compare

https://doi.org/10.1021/acssuschemeng.2c05326
ACS Sustainable Chem. Eng. 2022, 10, 15622−15641

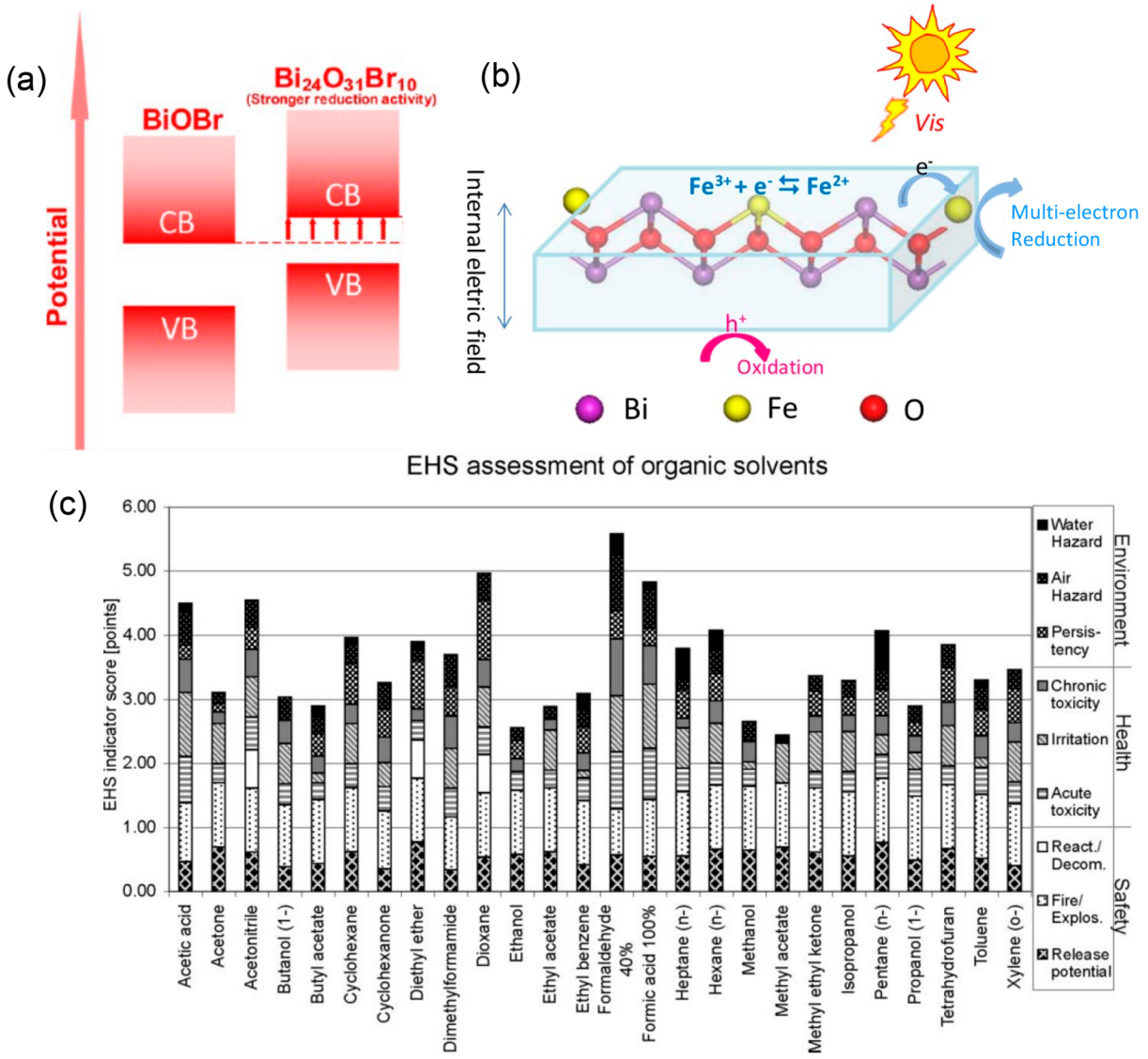

Figure 6. (a) Comparison of the band structures of BiOBr and bismuth-rich oxyhalide, $Bi_{24}O_{31}Br_{10}$. Adapted with permission from ref 99. Copyright 2014, American Chemical Society. (b) Schematic diagram of the photocatalysis process over the Fe(III)-modified BiOCl nanosheet visible light irradiation. Reproduced with permission from ref 102. Copyright 2016, Elsevier. (c) EHS scores for 26 organic solvents in the framework for the assessment of green solvents. The EHS score is composed of environmental indicators (water and air hazard, persistency), as well as indicators for health (chronic and acute toxicity and irritation) and safety (reaction/decomposition, fire/explosion, release potential) hazards. Reproduced with permission from ref 103. Copyright 2007, Royal Society of Chemistry.

with other methods, but their ultimate environmental impacts depend again on the reagents/template used, solvent system, and application of heat/pressure. Thus, we rank the first three methods in order of hydrolysis < hydrothermal < solvothermal, from least to most environmentally harmful.

We can look to the literature for LCA analyses of synthetic methods of other materials.[82−85] Ntouros et al. explored five synthetic routes toward ZIF-8 nanomaterials.[82] They showed that the use of methanol as a solvent accounts for 35% of the mean environmental impact, while this metric increases to 58% using DMF as a solvent. The use of deionized water as a solvent resulted in only 2% of the mean environmental impact, showing the negative impact of nonaqueous solvents. Wu et al. evaluated seven routes to TiO_2 nanoparticles across physical, chemical, and biological space.[85] Across all 10 impact categories measured (including GWP, fossil fuel depletion, and ecotoxicity), the sol−gel route (similar to hydrolysis methods discussed previously) was less impactful than hydrothermal syntheses, which were less impactful than solvothermal methods, consistent with the trend we presented.

Finally, we must acknowledge the differences in the resulting materials produced by the synthesis methods presented in this section. Using a functional unit of 1 kg BiOCl, the effects of the structural features on photocatalytic activity are not explored within this context but are important to the use stage analysis of BiOX sustainability. As outlined in the Characterization/Use Phase section, often the materials prepared by the least sustainable methods perform best in application, highlighting a balance that must be struck. With a different functional unit such as material surface area (enough material to have 1 m^2 of material surface exposed) or photocatalytic performance (enough material to produce 1 μmol H_2 per h), the conclusions drawn here may differ.

https://doi.org/10.1021/acssuschemeng.2c05326
ACS Sustainable Chem. Eng. 2022, 10, 15622−15641

CHARACTERIZATION/USE PHASE

$Bi_aO_bX_c$ (X = Cl, Br, I) materials with 2D layered structures have gained a lot of attention toward solar-to-chemical energy conversion, due to their enhanced optoelectronic properties compared to many oxide photocatalysts.[86] In addition, the strong internal static electric fields along the *c*-axis facilitate the effective separation of the photoinduced charge carriers.[87] Zhang et al. conducted the first investigation of the photocatalytic activity of an oxyhalide.[88] BiOCl was prepared by hydrolysis, and evaluation of the photodecomposition of methyl orange revealed that BiOCl exhibits better performance than TiO_2 (P25, Degussa) in aqueous medium under UV irradiation. However, the poor absorption of visible light due to the wide band gap of BiOCl limits its sustainability and commercial photocatalytic applications. The band gap of BiOX (X = Cl, Br, I) can be narrowed with larger halides, from BiOCl (3.2 eV), BiOBr (2.7 eV), to BiOI (1.7 eV), leading to more efficient visible light absorption.[89] The VBM of each of these oxyhalides makes the OER favored. Unfortunately, the positive CB position of BiOX (X= Cl, Br, I) makes them unsuitable for photocatalytic H_2 evolution (PHE). For PHE to take place, the conduction band minima should be more negative than the redox potential of H^+/H_2 (H_2/H^+= 0.00 V vs NHE at pH 0).[90] In order to obtain efficient PHE, the conduction band edge of BiOX materials needs to be shifted to more negative voltages. This challenge has been addressed in the literature by tuning the $Bi_aO_bX_c$ composition. As has been shown, many bismuth-rich $Bi_aO_bX_c$ materials have the capacity to perform overall water splitting. Other methods toward efficient overall water splitting include the formation of heterostructures which combine $Bi_aO_bX_c$ materials with a second absorbing material more suited toward HER. Both of these strategies and more will be discussed below. Currently, the reported photocatalytic approaches for H_2 production are more focused on superior performance, especially using sacrificial reagents or foreign elements as dopants or cocatalysts compared to the bare photocatalysts. In this section, we focus on evaluating the sustainability of different strategies employed to impart superior photocatalytic H_2 evolution efficiency to bismuth oxyhalide materials, namely, composition, crystal size, shape, faceting, and heterostructures. We also discuss the sustainability of the use phase of a photocatalyst's life cycle.

Composition. Adding cocatalysts, altering stoichiometry, introducing dopants, and developing multimetallic oxyhalides are some of the commonly used strategies for band structure engineering. While these methods primarily aim toward superior photocatalytic performance, this section evaluates the sustainability of the composition-based modifications on $Bi_aO_bX_c$ (X = Cl, Br, I) materials toward PHE.

Strong adsorption of H_2 on $Bi_aO_bX_c$ materials makes it difficult to evolve H_2 in an efficient manner. Strategies involving cocatalyst loading on the surface of the material have been used to tackle this problem and further boost the efficiency of photocatalysts.[91] Photoabsorbing materials like bismuth oxyhalides are good at generating electron−hole pairs, but usually do not have the ideal surface adsorption energies to facilitate water splitting redox reactions. Cocatalysts like noble metals can be used to provide appropriate reaction sites with ideal adsorption energies for carrying out photocatalytic processes. Additionally, the lower Fermi levels of noble metals when compared to those of photocatalysts can lead to the transfer of photoexcited electrons from the CB to the deposited metal.[92] Suitable Gibbs adsorption energies of H atoms (ΔG_H) can also lead to efficient PHE.[93] In particular, 1 wt % Pt was observed to be a good cocatalyst as it minimized the charge carrier recombination rate and provided an ideal surface for HER reactions.[78,94−96] In addition, cocatalysts can prevent photocorrosion of materials by timely consumption of photogenerated charges.[97] Noble metals, however, are not earth abundant and are costly, leading to sustainability concerns. Investigations into these problems have led to the discovery of many useful transition metal cocatalysts that are considerably more sustainable. For instance, metallic Bi acts as a cocatalyst to improve the PHE in $Bi/Bi_5O_7I/Sn_3O_4$ compared to the unmodified photocatalyst.[98] The PHE of the material was up to 326 μmol h^{-1} g^{-1}, which was 5 times higher than that of Sn_3O_4. If the loaded cocatalyst is earth abundant, cheap, nontoxic, enhances PHE, and can be recycled/reused, then the strategy of loading cocatalysts onto bismuth oxyhalides will enhance the overall material's sustainability.

The PHE of bismuth oxyhalides can also be boosted by fabricating bismuth-rich oxyhalides.[80,99] Since the CB position of BiOX is mainly composed of the bismuth 6*p* orbitals, adjustment of the bismuth content can modulate the CB position of BiOX as shown in Figure 6a.[99] For example, $Bi_{24}O_{31}Br_{10}$ has a negative CB position relative to the BiOBr CB position and thus a stronger reducing ability of the photogenerated electrons. The uplifting of the CBM is due to the bismuth 6*p* and Br 4*s* orbital hybridization resulting from the stoichiometry of elements.[99] Furthermore, *sp* hybridization leads to highly dispersive band structures, leading to lower effective masses of electrons and holes, which makes photoinduced charge carrier transfer more efficient.[100] There is greater tunability of surface atomic types, atomic quantities, and atomic distances in bismuth-rich materials compared to pristine BiOX.[22] The tunability of these parameters enables the feasibility of using the material for diverse applications. Apart from these advantages, the larger interlayer spacings and dipole moments of the bismuth-rich materials result in better polarization spaces and polarization forces, leading to larger internal electric fields, which minimize recombination of photogenerated electron−hole pairs.[28] Thus, the bismuth-rich strategy enables good n-type conductivity, larger intrinsic internal electric field, improved stability, enhanced photoreduction ability, and better harvesting of visible light in comparison to BiOX.[101] A chemical precipitation method was used to synthesize the $Bi_{24}O_{31}Br_{10}$ material by combining an acidic bismuth nitrate solution with a basic surfactant solution to control pH. The use of this material for PHE resulted in the generation of 66.95 μmol h^{-1} g^{-1} of H_2 under visible light irradiation. The constant PHE driven by visible light over long durations of time (experiment was conducted over a 5-day period) is promising in terms of sustainable use of the photocatalyst. The disadvantages stem from the usage of multiple reagents including $Bi(NO_3)_3{\cdot}5H_2O$, HNO_3, NaOH, and hexadecyltrimethylammonium bromide for the synthesis of the material, requirement for high temperature of about 500 °C for postannealing, and use of methanol as a sacrificial reagent during PHE.

Using a similar strategy, Bai et al. developed $Bi_4O_5X_2$ (X = Br, I) nanosheets with {101} facet exposure using a molecular precursor hydrolysis route, which was then further loaded with 1 wt % Pt as the cocatalyst by an *in situ* photodeposition method.[80] The few-layered structure of $Bi_4O_5X_2$ nanosheets can induce strong internal electric fields, resulting in high photoinduced

https://doi.org/10.1021/acssuschemeng.2c05326
ACS Sustainable Chem. Eng. 2022, 10, 15622−15641

carrier separation efficiency, leading to efficient PHE. $Bi_4O_5Br_2$ yielded a PHE of 167.5 μmol h^{-1} g^{-1} with an apparent quantum efficiency of 0.93% at 420 nm. However, $Bi_4O_5I_2$ displayed a lower photoinduced carrier separation efficiency than $Bi_4O_5Br_2$, resulting in a slightly lower PHE rate of 101.25 μmol h^{-1} g^{-1} with an apparent quantum efficiency of 0.52% at 420 nm. Although the material shows stable PHE over the course of 4 h, the durabilities of the photocatalysts for further elongated periods were not reported. Another disadvantage affecting sustainability is the usage of methanol as a sacrificial reagent during PHE and the requirement for an elongated period of heating at 160 °C for 16 h for the synthesis of a complex precursor. Along with this, a noble metal cocatalyst increases the activity but lessens the material's sustainability. As the photocatalyst is synthesized and further modified, the chemicals and energy used can contribute significantly to their environmental impact. Therefore, the substitution of the precursor materials and organic solvents with the greatest impact for another with less impact should be evaluated for the sustainable application of material toward PHE.[104] For instance, the environmental, health, and safety (EHS) assessment for the 26 pure organic solvents are given in Figure 6b.[103] Good candidates as "green solvents" include methyl acetate, ethanol, and methanol, having low scores due to their particularly low environmental and health hazards, whereas formaldehyde, dioxane, formic acid, acetonitrile, and acetic acid possess overall high scores, making them less sustainable solvents. If a synthesis technique with a less environmentally impactful solvent can be developed to modulate composition and perform stable PHE without any sacrificial reagents or cocatalysts for elongated durations of time, it can be one of the most sustainable ways to achieve band structure engineering.

Doping with foreign elements is an efficient path to tune the electronic structure, enhance the wettability properties, reduce the kinetic energy barrier, and introduce additional active sites, which will lead to improved photocatalytic activity.[105] By doping, additional energy levels can be introduced into the band structure, which can be used to trap photogenerated electrons and holes to minimize charge carrier recombination.[106] In this way, photogenerated charge carriers lifetimes can be lengthened by doping, resulting in an increased photocatalytic activity. The synergistic effect of doping could confer the photocatalyst with improved morphological characteristics, increased specific surface area, optimal light absorption capability, enhanced charge transfer, suppressed charge carrier recombination, and an increased amount of surface oxygen vacancies.[107,108] The oxygen vacancies can act as trap states for CB electrons curtailing direct recombination of charge carriers and additionally serve as active sites to accelerate surface redox kinetics.[109] Importantly, photocatalytic dopants should be selected such that they are earth abundant and made of nontoxic elements in order to achieve greater sustainabilities. A balance must be struck between improved PHE performance and potential adverse environmental impacts introduced by doping.[104]

Li et al. observed that homogeneous carbon doping led to enhanced PHE with BiOCl nanosheets having high exposure of {001} or {010} facets.[110] Specifically, the carbon-doped BiOCl material was optimally loaded with a 3 wt % NiO_x cocatalyst and evaluated in the presence of triethanolamine (a hole scavenger) under simulated solar light irradiation. Homogeneous carbon doping enhanced the PHE rate by a factor of 3.6 (to 240 μmol h^{-1} g^{-1}) for {001}-faceted BiOCl nanosheets and by a factor of 8.1 (to 420 μmol h^{-1} g^{-1}) for {010}-faceted BiOCl nanosheets. There was a strong correlation between the final carbon doping amounts in the BiOCl nanosheets and the resulting specific facet exposure. Doping of the photocatalyst with an abundant nonmetal like carbon makes the method attractive in terms of sustainability. In addition, using a NiO_x cocatalyst is a good choice as Ni is an earth abundant metal.

Mi et al. hydrothermally synthesized Fe(III)-doped BiOCl ultrathin nanosheets.[102] Fe(III) doping and surface grafting facilitate the interfacial charge transfer as well as narrow the band gap compared to undoped BiOCl. In addition, the self-induced electric field within BiOCl nanosheets, along with its five atomic layer thickness could efficiently enhance the separations and transfer efficiencies of charge carriers. A scheme of the proposed photocatalysis process is shown in Figure 6c. The trap levels from doping with Fe(III) allow for excitation of electrons under visible light irradiation. The static internal electric field due to the characteristic layered structure of BiOCl and the shortened transport route offered by the thin nanosheet morphology can enable the facile separation and transfer of the photogenerated electrons and holes to the surfaces of the nanosheets to mediate the surface redox reactions. The Fe(III)-doped BiOCl nanosheets displayed a PHE rate of 141.6 μmol h^{-1} g^{-1} under visible light irradiation for 8 h, whereas the undoped sample exhibited a PHE rate of about 62.4 μmol h^{-1} g^{-1} under the same conditions. The doping resulted in an increase in PHE by ~2.3 times compared to the undoped sample, and the long-term PHE demonstrates the photocatalytic stability of the material. Given the earth abundant nature of the dopant and increased PHE, Fe doping improves the sustainability of the material.

Recent studies have revealed that multimetallic oxyhalide materials such as Bi_4MO_8X (M = Nb, Ta; X = Cl, Br) are attractive photocatalysts for water splitting.[111−115] The unit cell of Bi_4MO_8X is composed of charged layers of fluorite-type $[Bi_2O_2]^{2+}$ intergrown with alternating layers of $[MO_4]^{3-}$ and $[X]^-$. Like BiOX, the alternating layers provide an internal static electric field, leading to effective charge separation. Destabilized O 2*p* orbitals, rather than halide orbitals, comprise the VBM as proposed by the revised lone pair (RLP) model.[116] According to the RLP model, filled bismuth 6*s* orbitals interact strongly with the filled O 2*p* states in the valence band, leading to filled antibonding orbitals that are stabilized by their interaction with bismuth 6*p* orbitals.[117] The result is a VBM composed mainly of O 2*p* orbitals which significantly curtails photooxidation of the halide ions ($2Cl^- + 2h^+ \rightarrow Cl_2$), thereby providing photostability over long operating conditions.[17]

Wei et al. synthesized the visible-light absorbing photocatalyst Bi_4MO_8X (M = Nb, Ta; X = Cl, Br)—a perovskite oxyhalide—*via* a solid-state method for efficient PHE.[111] The best PHE (98.3 μmol h^{-1} g^{-1}) was observed for Bi_4NbO_8Br when glycerol was used as a sacrificial reagent and Pt as a cocatalyst under simulated sunlight (300 W Xe lamp). The superior PHE of niobium-based samples compared to the tantalum-based samples could be attributed to the lower twisting degree of the $[Bi_2O_2]^{2+}$ layer which is favorable for the mobility of the photocarriers. When the same experiment was conducted under visible light irradiation (>420 nm), the Bi_4NbO_8Br photocatalyst yielded a PHE rate of 83.3 μmol h^{-1} g^{-1} with a quantum efficiency of 0.4%, which was larger than for typical bismuth-based oxyhalides (0% for both BiOCl and BiOBr). This achievement is commendable since more than 40% of the solar spectrum is visible light, while UV-light only represents 4%.[111] Of course, these advances in visible light absorption and

https://doi.org/10.1021/acssuschemeng.2c05326
ACS Sustainable Chem. Eng. 2022, 10, 15622−15641

durability must be weighed against the sustainability of the added metals and increased synthetic complexity.

Crystal Size, Shape, and Faceting. By controlling crystal sizes, shapes, and/or facetings of BiOX materials, a single platform can be provided to control the reactivity and selectivity of a photocatalyst by controlling its physicochemical properties.[118] For instance, constructing nanostructures can minimize the charge carrier traveling distance to reach the surface of the material, minimizing recombination and aiding in better PHE. Photocatalytic reactivity varies among exposed surfaces due to the anisotropic layered structure. $Bi_aO_bCl_c$ materials can potentially have surfaces terminate with layers expressing Bi, O, or Cl. Thermodynamic calculations have revealed that O terminations are most stable for the {001} facets of BiOCl rather than Cl or Bi terminations.[119] On the edges of the layers ({010} facets of BiOCl, for example), the surface termination is less definite. Crystal facet engineering can efficiently modulate atomic rearrangement and coordination and hence result in different surface electronic structures, electrical conductivity, reaction centers, and reactant adsorption sites.[118]

Ye et al. have synthesized black ultrathin BiOCl nanosheets in a glycerol-based system.[87] The alcohol groups in glycerol can react with the exposed oxygen on the {001} surfaces of BiOCl, leading to the formation of oxygen vacancies that can lead to high PHE. On the other hand, the high viscosity of glycerol can affect ion diffusion efficiency, resulting in the formation of the 2D BiOCl nanosheets with thicknesses of ∼3 nm. The expanded *d*-spacings of the {001} crystal planes and oxygen vacancies of the photocatalyst enhanced the internal electric field intensity, separation of charge carriers, and photon absorption efficiency. In addition to these advantages, the higher CBM and lower VBM of ultrathin samples when compared to bulk BiOCl can result in higher oxidizing and reducing powers of photogenerated holes and electrons, respectively. These nanosheets showed enhanced PHE activity (50.2 μmol h^{-1} g^{-1}) when compared to bulk BiOCl (2.4 μmol h^{-1} g^{-1}) under $\lambda \geq 420$ nm light irradiation for 5 h in the presence of 10 vol % triethanolamine as a hole scavenger.[87] The photocatalyst can perform efficient PHE even without any cocatalyst, making it a suitable candidate for sustainable photocatalysis. Loading Pt as cocatalyst led to further enhancement of PHE (79.2 μmol h^{-1} g^{-1}). The repeatability was also very excellent with these ultrathin nanosheets, exhibiting PHE activity of 49.6 μmol h^{-1} g^{-1}. One drawback of the synthesis technique is the requirement of heating at 160 °C for 16 h.

Likewise, Zhang et al. synthesized ultrathin BiOCl nanosheets with surface/subsurface defects toward solar-driven water splitting using a shorter duration of solvothermal heating (160 °C for 4 h).[90] The layered crystal structure of BiOCl inherently favors plate-like morphologies with large {001} facets, but the addition of polyvinylpyrrolidone (PVP) into the mannitol-based solvothermal synthesis promotes the formation of ultrathin nanosheets. PVP serves as a surfactant and shape controlling agent restricting growth along the *c*-axis. Ultrathin BiOCl nanosheets of thicknesses of ∼3.6 nm were used for PHE under 500 W Xe light irradiation resulting in the production of 34.8 μmol h^{-1} g^{-1} of H_2 gas. Photocatalytic stability was observed also for the same conditions over multiple cycles of PHE. Moreover, no obvious activity loss was observed for as long as 100 days. Excitingly, no cocatalysts or sacrificial reagents were required, providing promise toward a sustainable BiOCl system. Density functional theory calculations showed that the oxygen vacancies in the ultrathin nanostructures facilitated H_2O adsorption, followed by dissociation and H_2 formation.

Hierarchical bismuth oxyhalides of the type BiOX with flower-like structures were synthesized by Lee et al. by a facile one-pot microwave-assisted solvothermal method using $Bi(NO_3)_3{\cdot}5H_2O$ along with ethylene glycol and ethanol as solvents.[120] The microwave-assisted solvothermal synthesis is superior over the conventional hydrothermal synthesis since the former method can elevate the rate of reaction by 1 to 2 orders of magnitude through rapid heating, and novel phases can be formed. Rapid heating along with rapid kinetics makes this method more sustainable due to plausible energy savings.[120,121] Other benefits arise from the hierarchical structure, including high surface area, thermal stability, enhanced photon absorption, and better diffusional ability. Notably, BiOI achieved a PHE rate of 1316.9 μmol h^{-1} g^{-1} under visible light irradiation without any hole scavenger or cocatalyst. The enhanced PHE is due to not only to reduced charge carrier recombination rates (lowest photoluminescence intensity), but also a more appropriate conduction band position to reduce H^+ to H_2 than the other BiOX congeners.

Di et al. have adopted another strategy based on tuning local atomic arrangement and electronic structure by tailoring surface defects.[33] They designed single unit cell thick Bi_3O_4Br nanosheets with unique surface defects, resulting in control of the local atomic arrangement and electronic structure, boosting PHE by about 4.9 times (380.0 μmol h^{-1} g^{-1}) when compared to bulk Bi_3O_4Br, due to the increased charge separation efficiency.[33] The atom-scale thicknesses and appearances of new defect levels uplifted the CB edge of the photocatalyst by ∼0.61 eV relative to that of bulk Bi_3O_4Br, leading to the production of more reductive photogenerated electrons to involve in PHE. Although the synthesis involves heating of precursors in an oven for an extended period (24 h at 160 °C), usage of 10 vol % methanol as a hole scavenger, and 1 wt % Pt as the cocatalyst, it is promising to have no significant activity loss of PHE after three cycles.

Pan et al. have conducted theoretical studies of Janus bismuth oxyhalide (Bi_2O_2XY, where X/Y = Cl, Br, or I, and X ≠ Y) with asymmetric halogen surfaces on both sides as shown in Figure 7a−c.[122] The Janus asymmetry induces an electrostatic potential difference, leading to a staggered band alignment, which enables efficient PHE. The strong internal electric field endowed by in-plane asymmetry of the 2D layered Janus materials was cited to provide efficient separation of the photogenerated charge carriers and improvement of the photocatalytic performance when compared to pristine BiOX. The smaller electronegativities of the terminal halogens lead to more suitable Gibbs free energies of hydrogen adsorption when compared to monohalogenated BiOX. Since the work done by Pan et al. entails theoretical studies, although superior PHE can be expected, the sustainability aspect cannot be fully evaluated. Nevertheless, the phonon spectra calculation of Janus Bi_2O_2ClBr, Bi_2O_2BrI, and Bi_2O_2ClI showed no imaginary frequencies, which supports the stabilities of the structures. In turn, these results suggest they may be prepared experimentally.

Heterostructures. A heterostructure consists of different materials which are physically or chemically bonded together, exhibiting a complex geometry and a distinct junction interface that ideally leads to superior performances of semiconductor heterostructures compared to the individual semiconductor materials.[124] Each component has its own crystal structure, potentially with different orientations, and when combined, a

https://doi.org/10.1021/acssuschemeng.2c05326
ACS Sustainable Chem. Eng. 2022, 10, 15622−15641

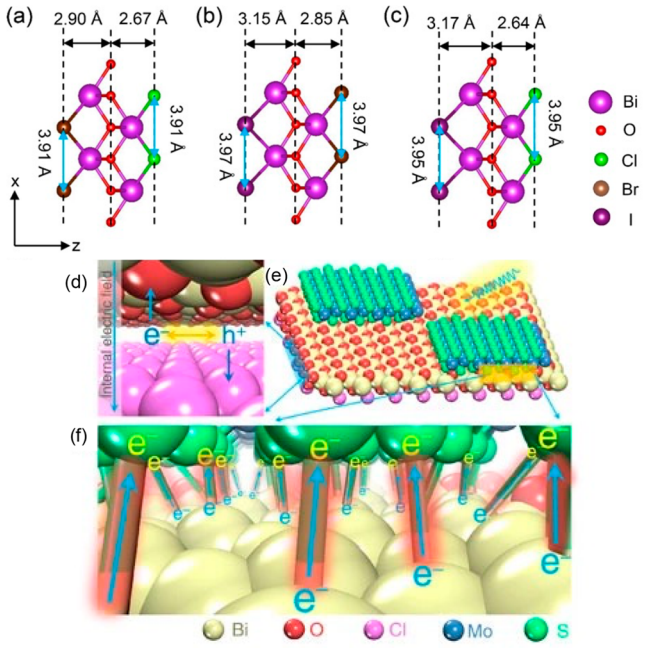

Figure 7. Layered structure monolayers of (a) Bi_2O_2ClBr, (b) Bi_2O_2BrI, and (c) Bi_2O_2ClI with distances between oxygen and halogen layers. Reproduced with permission from ref 122. Copyright 2022, Elsevier. Schematic illustration of the crystal structure of $Bi_{12}O_{17}Cl_2$-MoS_2 (d) and of the charge flow processes within $Bi_{12}O_{17}Cl_2$-MoS_2, including the electron−hole separation within monolayer $Bi_{12}O_{17}Cl_2$ (e) and the interfacial electron transfer from monolayer $Bi_{12}O_{17}Cl_2$ to monolayer MoS_2 along the Bi−S bonds (f). Reproduced from ref 123 which has a Creative Commons Attribution 4.0 International License, published by Springer Nature.

distinct interface with different energy alignments is formed.[118] Proper band alignment at the interface between the two components of a heterostructure is crucial for interfacial charge transfer and separation. Type-II band heterostructures are extensively studied for photocatalytic applications. A typical type-II heterojunction has staggered band gap energies, with the conduction and valence bands energies of one semiconductor relatively higher than the other semiconductor. This alignment leads to photoexcited electrons and holes being driven in opposite directions, separating the two redox half reactions and leading to minimized recombination and outstanding solar conversion efficiency.[125]

Kandi et al. modified BiOI microplates with CdS quantum dots (QDs) for efficient PHE under visible light irradiation.[126] CdS QDs are capable of allowing multiple exciton generations from a single photon and has a band gap that is tunable by its size, maximizing the range of visible light absorption. Unfortunately, CdS QDs cannot be used as a standalone photocatalyst due to self-oxidation. This problem can be resolved by creating composites with BiOI microplates. Further, the composite enhances the separation of electron−hole pairs through the type-II heterostructure band alignment, leading to PHE at the CdS surface. Among the photocatalysts studied, the 4% CdS QDs/BiOI composite generated 4060 μmol h^{-1} g^{-1} of H_2 under visible light irradiation. The BiOI microplates were prepared by a simple hydrolysis method, while the CdS QDs were synthesized using a two-step precipitation deposition method. Although photocatalytic experiments involved 10 vol % methanol solution as the hole scavenger, absence of any additional cocatalyst is beneficial toward sustainability. Even though very high efficiency for PHE under visible light irradiation was achieved, one disadvantage is the use of thioglycolic acid as a capping agent for prevention of agglomeration of the extremely small QDs. Thioglycolic acid is reported to be a chemical of high toxicity, which can be absorbed through skin and cause damage to organs or systems in animals.[127] In addition, CdS itself can be cytotoxic.[128] To circumvent these limitations, biocompatible biopolymers like chitosan can be used to modify CdS. These biopolymers improve QD solubility and lessen the cytotoxicity of xenobiotic elements such cadmium ions while maintaining photocatalytic properties.[129]

Li et al. have crafted Janus $Bi_{12}O_{17}Cl_2$-MoS_2 bilayer junctions as a new 2D motif.[123] A facile hydrothermal process resulted in oriented anchoring of MoS_2 monolayers on the $[Bi_{12}O_{17}]^{2+}$ layer of $Bi_{12}O_{17}Cl_2$. The key to the assembly is the metallic characteristics of MoS_2 monolayers and the asymmetric structure of $Bi_{12}O_{17}Cl_2$ composed of $[Cl_2]^{2-}$ layers and oxygen deficient $[Bi_{12}O_{17}]^{2+}$ layers. Atomic-level directional charge separation is possible due to the internal electric field created between the $[Bi_{12}O_{17}]^{2+}$ and $[Cl_2]^{2-}$ end faces (Figure 7d−f), resulting in the flow of electrons to $[Bi_{12}O_{17}]^{2+}$ end faces.[123] In addition, Bi−S bonds formed between the $[Bi_{12}O_{17}]^{2+}$ and MoS_2 monolayers enable further electron migration to MoS_2 for PHE to take place. The more negative CBM of $Bi_{12}O_{17}Cl_2$ compared to MoS_2 suggests that electron transfer from $[Bi_{12}O_{17}]^{2+}$ to MoS_2 is thermodynamically favorable. The internal electric field also drives holes to the $[Cl_2]^{2-}$ layer, leading to the oxidation of the organic scavengers (ascorbic acid). Steering of charge flows endows the material with an ultralong carrier lifetime of 3446 ns and hence a remarkable PHE rate of 33,000 μmol h^{-1} g^{-1} and a quantum yield of around 36% under visible light irradiation. The exceptional PHE and stability in activity over 100 h of light irradiation indicates the robustness of the photocatalyst.

END OF LIFE

The largest share of a material's environmental impact is often in the other phases beyond the use phase.[130] Therefore, plans must be made for what happens to the used bismuth oxyhalides at the end of the photocatalyst life cycle. Sustainable methods to reuse, recycle, or repurpose the waste can minimize the potential wide-ranging harmful effects of the material's life cycle. Unfortunately, these areas are the least developed of all for bismuth oxyhalides. Currently, less than 1% of bismuth is recycled.[131,132] Recycling bismuth has proven challenging due to its use in dissipative applications (i.e., pigments, cosmetics, and pharmaceuticals). Efforts to recycle bismuth have increased since the European Commission classified it a critical raw material in 2017 and the USA designated it a critical mineral in 2018.[47,132] Part of the motivation for improved recycling of bismuth is the fact that nearly 100% of USA and European demand for bismuth is met by imported sources, mainly from China.[131] This sourcing bottleneck can be ameliorated by diversifying the raw material supply to include recycled bismuth sources.

Alongside developing photocatalytic bismuth oxyhalides from pristine reagents, we should also promote the synthesis of such materials using degraded materials. These can include bismuth oxyhalides with halide deficiencies after leaching and particles with poor morphologies being restored to their optimal conditions. Incorporating bismuth oxyhalides into existing supply chains would also be sustainable, such as used photocatalysts being sold as pigments. Improved recycling and reusing of bismuth materials would lessen the need for virgin

https://doi.org/10.1021/acssuschemeng.2c05326
ACS Sustainable Chem. Eng. 2022, 10, 15622−15641

bismuth ore mining which is inherently tied to toxic lead production as described in the Raw Materials section. If refurbishment or reuse is not feasible, an ideal end of life process would be to reintroduce the material back into the environment in a harmless, safe manner.

The toxicity of bismuth oxyhalides entering the environment must also be considered. Bismuth is generally immobile in the soil as it forms solid bismuth oxides and hydroxides.[45] Further, bismuth is nontoxic to humans and poses a minimal threat to the environment. Potentially more dangerous is the downstream effect of halide ions and secondary metals. Halide ions can gradually be leached from bismuth oxyhalide materials and due to their high solubility can spread quickly. Halides are found naturally in the environment; however, these anions can become toxic to aquatic organisms at high levels as has been shown in runoff after winter road salt application.[133]

As an aside, major end of life concerns have been discussed regarding silicon photovoltaic (PV) waste. As the PV industry is farther ahead toward commercialization and global implementation than photocatalysis, we can look at the issues faced by the PV community to anticipate future challenges to photocatalysis and address them proactively rather than reactively. A 2022 C&EN article highlighted this issue, warning that 8 million tons of PV waste will be generated by 2030 and 80 million tons by 2050.[134−136] This waste is of great concern not only for the loss of valuable materials (silver, copper, and high purity silicon), but for the release of toxic components like lead.[137] In the USA, a lack of federal regulations addressing PV recycling has caused a recycling rate of <10%, and even when "recycled", the bulk materials by mass like aluminum frames and glass are often only repurposed. The rest, which contains two-thirds of the monetary value is commonly incinerated. Since half the energy utilized in PV production goes toward producing the solar module, recycling these components would significantly improve the material's sustainability. Other reviews and LCAs properly address recycling issues with PV systems in depth.[138−141] We highlight this topic to learn and anticipate what may be to come regarding photocatalyst waste, including bismuth oxyhalides.

Solutions that can be implemented now during the design and research and development phases include funding innovative businesses that address sustainability of emerging materials and legislating recycling programs. The USA state of Washington has initiated new regulations requiring companies to have state-approved plans for end of life care before producing or selling any PV modules.[142] Such an example directly ties together product commercialization with end of life sustainability. As scientists, we too can contribute to these efforts by addressing the end of life sustainability of our approaches in our novel research publications.[143] We must ask the question, who is responsible for these issues? At the core, we are responsible for the materials that we produce and sell. This stewardship must not end at the point of sale but also include the eventual end of life stage of a product.

CONCLUSION AND PERSPECTIVE

Bismuth oxyhalides are a promising class of layered materials with photocatalytic applications toward H_2 production. Bismuth oxyhalides are advantageous due to their compositional flexibilities, nontoxic natures, and layered crystal structures. The layered structure allows photogenerated holes and electrons to be spatially separated into the charged layers of the crystal structures, leading to longer charge carrier lifetimes and diminished recombination. The potential of bismuth oxyhalides as a solution to the energy crisis requires that we also evaluate them on their sustainability. Through this Perspective, we have detailed the sustainability of bismuth oxyhalide systems at each stage across its cradle to grave life cycle.

The sustainability of the raw material stage is dominated by bismuth's intricate relationship with lead and lead's toxicity. To use bismuth oxyhalides as photocatalysts on a global scale, the production of refined bismuth must be sustainable. This indicates that bismuth production must be separated from lead production as much as possible. As the world transitions further away from the use of lead, there may come necessary changes where bismuth ores are mined and how it is refined and purified. Metallurgic research should be directed toward finding new ways to maximize sustainable bismuth production with minimal harmful byproducts such as lead. As the overwhelming majority of the GWP and CED of bismuth production comes in the refinement and purification stages, improvements of these sustainability "bottlenecks" will be paramount. The United States is almost fully reliant on bismuth imports and maintains no government stockpile. Therefore, strong international political and industrial relationships will be crucial to maintain fair, economical, and sustainable access to bismuth broadly.

The most sustainable methods to synthesize bismuth oxyhalides use minimal energy inputs such as heat, water as the solvent, and sustainable cocatalysts and additives. Since bismuth oxyhalides can be produced simply at room temperature with hydrolysis methods, the benefits of additional energy/resource inputs, processing steps, and postsynthetic modifications must be weighed against the lower sustainability of these actions. For example, templated methods to synthesize bismuth oxyhalides should weigh the overall performance improvement imparted by the template against the sustainability of producing and using the template. Among the directly comparable synthesis methods discussed, we find hydrolysis methods to be more sustainable than hydrothermal methods, which are more sustainable than solvothermal methods. This is *not* to say that there is no value in researching hydrothermal and/or solvothermal methods, but rather that these extra steps must be evaluated to be worth performing in terms of the overall sustainability and offset with improvements in PHE.

Improvements to the PHE of bismuth oxyhalides can be imparted further by modifications to the materials' crystal sizes, shapes, facetings, compositions, and architectures. These modifications each affect the product's ultimate sustainability. Doping or inclusion of an additional element into the structure can have major effects on the material's electronic properties and overall stability. Formation of heterostructures and cocatalyst loading of bismuth oxyhalides with other materials can lead to improved charge carrier separation and add superior surfaces to facilitate surface redox reactions. Because of the nature of these modifications from pure bismuth oxyhalides, the sustainability of each is hard to compare. We make a similar conclusion to that of the Comparative Sustainability of Synthesis Methods section, namely, that the sustainability "cost" of additives or strict synthesis conditions required to modify the size, shape, faceting, composition, and architecture must be outweighed by improved performance of the material enough to justify their use.

The end of the material's life represents the largest area for sustainability improvements. As less than 1% of bismuth is currently recycled, the development of processes to reuse, recycle, and repurpose spent bismuth oxyhalide photocatalyst materials is critical.[131,132] This emphasis will also reduce the significance of the raw material stage with time. As most

https://doi.org/10.1021/acssuschemeng.2c05326
ACS Sustainable Chem. Eng. 2022, 10, 15622−15641

photocatalysts degrade with use, having a method to regenerate an active photocatalyst or an application where used bismuth oxyhalides can be repurposed will limit the need to process and refine more bismuth ores. Researchers should attempt to produce quality photocatalytic materials from degraded materials. Advancements in this area have the potential to transform the viability of using bismuth oxyhalides as photocatalysts for H_2 production.

The conclusion and perspective we present is not absolute. Researchers are encouraged to refine and provide new ideas and solutions to fast-track bismuth oxyhalides as a sustainable solution to the energy crisis. We note that our life cycle assessment lacks quantitative data at many key process steps. We hope future researchers will help fill these gaps to visualize a more complete picture of the life cycle assessment of bismuth oxyhalides.

Looking forward, the future development of bismuth oxyhalides for photocatalytic H_2 production is bright. Research into synthetic control of the materials' crystal sizes, shapes, facetings, compositions, and architectures, as well as research into postsynthetic modifications with cocatalysts and heterostructures, will be key to maximize performance metrics including H_2 production. Future developments can also address bismuth oxyhalide limitations, such as its photostability and CBM positioning. As these materials near commercialization, device development and fabrication will play important roles as well. All this future work, however, must include sustainability considerations at each stage.

Reviewing recent literature in the field of bismuth oxyhalides shows that this area continues to expand *via* demonstrations of enhanced performance metrics and new synthetic routes with structural control; however, there is a noticeable lack of consideration for the sustainability of these materials. By exploring the life cycle of bismuth oxyhalides, we hope to initiate more conversation in the field and encourage researchers to assess the sustainability of their own work in future publications. Further improvement of performance metrics is valuable, but only within a deeper context in which sustainability is evaluated concomitantly. By including sustainability alongside performance assessments in future publications, researchers will then be able to compare diverse materials to find the best candidates for *sustainable* and *efficient* photocatalysts for H_2 production.

AUTHOR INFORMATION

Corresponding Author

Sara E. Skrabalak − *Department of Chemistry, Indiana University, Bloomington, Indiana 47405, United States;* orcid.org/0000-0002-1873-100X; Email: sskrabal@indiana.edu

Authors

Matthew N. Gordon − *Department of Chemistry, Indiana University, Bloomington, Indiana 47405, United States;* orcid.org/0000-0001-7212-9047

Kaustav Chatterjee − *Department of Chemistry, Indiana University, Bloomington, Indiana 47405, United States;* orcid.org/0000-0003-3527-9796

Nayana Christudas Beena − *Department of Chemistry, Indiana University, Bloomington, Indiana 47405, United States;* orcid.org/0000-0001-9603-5475

Complete contact information is available at: https://pubs.acs.org/10.1021/acssuschemeng.2c05326

Author Contributions

K.C. and N.C.B contributed equally. The manuscript was written through the contributions of all authors. M.N.G. conceptualized and wrote substantial portions of the manuscript, while managing the team writing process with oversight and feedback from S.E.S. K.C. and N.C.B. contributed equally, with K.C. contributing substantially to the introduction, bismuth oxyhalides ($Bi_aO_bX_c$), and $Bi_aO_bX_c$ materials production sections and N.C.B. contributing substantially to the raw materials and characterization/use phase sections. All authors have given approval to the final version of the manuscript.

Funding

This work was supported by Indiana University and US NSF DMR-2113536.

Notes

The authors declare no competing financial interest.

Biographies

Matthew N. Gordon is a Ph.D. candidate in the Skrabalak group at Indiana University−Bloomington. He received his B.S. degree in chemistry from The Ohio State University in 2014 where he conducted research with Prof. Yiying Wu. After working in the pharmaceutical industry for a few years, he began his Ph.D. studies in 2017 at IU. Matt is researching novel precursors for photocatalytic materials.

Kaustav Chatterjee is being advised for his Ph.D. in the laboratory led by Professor Sara E. Skrabalak at Indiana University−Bloomington. In 2018, he received his M.S. degree in chemistry from the Indian Institute of Science Education and Research (IISER) Mohali, India, having completed in 2015 his B.Sc. (Honours) degree in chemistry from St. Xavier's College, Kolkata, India. His M.S. research with Professor Ujjal K. Gautam involved the use of semiconductors in the conversion of toxic pollutants to value-added chemicals. His current research interests are on developing novel and durable multimetallic semiconductor

https://doi.org/10.1021/acssuschemeng.2c05326
ACS Sustainable Chem. Eng. 2022, 10, 15622−15641

photocatalysts for solar energy harvesting applications and elucidating their structure−property correlations.

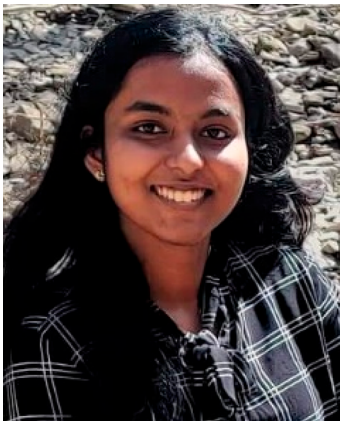

Nayana Christudas Beena is a Ph.D. candidate from the Chemistry Department at Indiana University−Bloomington, working with Prof. Sara E. Skrabalak. Nayana received her integrated B.S.−M.S. dual degree in chemistry in 2019 from Indian Institute of Science Education and Research, Mohali, where she worked on the shape selective synthesis of palladium nanostructures for improved catalytic applications, such as Suzuki cross-coupling reactions and nitrophenol reduction, with Prof. Ujjal K Gautam. She joined Indiana University − Bloomington in 2019. Her current research focuses on identifying novel multimetallic metal oxyhalide intergrowths capable of visible light absorption that are also durable against photocorrosion, allowing for sustained photocatalysis.

Sara Skrabalak is a James H. Rudy Professor at Indiana University−Bloomington, where she began her career in the Chemistry Department in 2008. She has received many awards, most recently being named a fellow of the American Association for the Advancement of Science in 2020. Professor Skrabalak is Editor-in-Chief for both *Chemistry of Materials* and *ACS Materials Letters*. Her research group develops new synthetic methods for nanomaterials for applications in catalysis, solar energy, chemical sensing, security, and more (https://skrablab.sitehost.iu.edu).

■ ACKNOWLEDGMENTS

The authors thank all researchers who have supported this project and contributed to the cited manuscripts.

■ REFERENCES

(1) Bossel, U.; Eliasson, B.; Taylor, G. The Future of the Hydrogen Economy: Bright or Bleak? *Cogeneration & Distributed Generation Journal* **2003**, *18*, 29−70.
(2) *The Future of Hydrogen: Seizing Today's Opportunities*; International Energy Agency, 2019.
(3) Rifkin, J.*The Hydrogen Economy: The Creation of the Worldwide Energy Web and the Redistribution of Power on Earth*; J. P. Tarcher/Putnam: New York, 2002; pp 1−294.
(4) Guy, K. W. A. The Hydrogen Economy. *Trans. Inst. Chem. Eng.* **2000**, *78*, 324−327.
(5) Staffell, I.; Scamman, D.; Velazquez Abad, A.; Balcombe, P.; Dodds, P. E.; Ekins, P.; Shah, N.; Ward, K. R. The role of hydrogen and fuel cells in the global energy system. *Energy Environ. Sci.* **2019**, *12*, 463−491.
(6) van Renssen, S. The hydrogen solution? *Nat. Clim. Change* **2020**, *10*, 799−801.
(7) Rosen, M. A.; Koohi-Fayegh, S. The prospects for hydrogen as an energy carrier: an overview of hydrogen energy and hydrogen energy systems. *Energy Ecol. Environ.* **2016**, *1*, 10−29.
(8) Brandon, N. P.; Kurban, Z. Clean energy and the hydrogen economy. *Philos. Trans. R. Soc., A* **2017**, *375*, 20160400.
(9) Eljack, F.; Kazi, M.-K. Prospects and Challenges of Green Hydrogen Economy via Multi-Sector Global Symbiosis in Qatar. *Front. Sustain.* **2021**, *1*, 612762.
(10) Wang, Q.; Domen, K. Particulate Photocatalysts for Light-Driven Water Splitting: Mechanisms, Challenges, and Design Strategies. *Chem. Rev.* **2020**, *120*, 919−985.
(11) *Road Map to a US Hydrogen Economy: Reducing Emmission and Driving Growth Across the Nation*; The Fuel Cell and Hydrogen Energy Association, 2020.
(12) *Global Hydrogen Review 2021*; International Energy Agency, 2021.
(13) Spath, P. L.; Mann, M. K.*Life Cycle Assessment of Renewable Hydrogen Production via Wind/Electrolysis: Milestone Completion Report*; National Renewable Energy Laboratory:, 2004.
(14) Mehmeti, A.; Angelis-Dimakis, A.; Arampatzis, G.; McPhail, S.; Ulgiati, S. Life Cycle Assessment and Water Footprint of Hydrogen Production Methods: From Conventional to Emerging Technologies. *Environments* **2018**, *5*, 24.
(15) Osman, A. I.; Mehta, N.; Elgarahy, A. M.; Hefny, M.; Al-Hinai, A.; Al-Muhtaseb, A. a. H.; Rooney, D. W. Hydrogen production, storage, utilisation and environmental impacts: a review. *Environ. Chem. Lett.* **2022**, *20*, 153−188.
(16) Zhao, G.; Pedersen, A. S. Life Cycle Assessment of Hydrogen Production and Consumption in an Isolated Territory. *Procedia CIRP* **2018**, *69*, 529−533.
(17) Chatterjee, K.; Skrabalak, S. E. Durable Metal Heteroanionic Photocatalysts. *ACS Appl. Mater. Interfaces* **2021**, *13*, 36670−36678.
(18) Cui, J.; Li, C.; Zhang, F. Development of Mixed-Anion Photocatalysts with Wide Visible-Light Absorption Bands for Solar Water Splitting. *ChemSusChem* **2019**, *12*, 1872−1888.
(19) Miyoshi, A.; Maeda, K. Recent Progress in Mixed-Anion Materials for Solar Fuel Production. *Sol. RRL* **2021**, *5*, 2000521.
(20) Di, J.; Xia, J.; Li, H.; Guo, S.; Dai, S. Bismuth oxyhalide layered materials for energy and environmental applications. *Nano Energy* **2017**, *41*, 172−192.
(21) Nakada, A.; Higashi, M.; Kimura, T.; Suzuki, H.; Kato, D.; Okajima, H.; Yamamoto, T.; Saeki, A.; Kageyama, H.; Abe, R. Band Engineering of Double-Layered Sillén-Aurivillius Perovskite Oxychlorides for Visible-Light-Driven Water Splitting. *Chem. Mater.* **2019**, *31*, 3419−3429.
(22) Xiong, J.; Song, P.; Di, J.; Li, H. Bismuth-rich bismuth oxyhalides: a new opportunity to trigger high-efficiency photocatalysis. *J. Mater. Chem. A* **2020**, *8*, 21434−21454.
(23) Biswas, A.; Das, R.; Dey, C.; Banerjee, R.; Poddar, P. Ligand-Free One-Step Synthesis of {001} Faceted Semiconducting BiOCl Single Crystals and Their Photocatalytic Activity. *Cryst. Growth Des.* **2014**, *14*, 236−239.
(24) Keller, E.; Ketterer, J.; Krämer, V. Crystal structure and twinning of $Bi_4O_5Br_2$. *Z. Kristallogr. - Cryst. Mater.* **2001**, *216*, 595−599.

https://doi.org/10.1021/acssuschemeng.2c05326
ACS Sustainable Chem. Eng. 2022, 10, 15622−15641

(25) Eggenweiler, U.; Keller, E.; Krämer, V.; Meyer, C. A.; Ketterer, J. Crystal structure of tribismuth tetraoxide chloride, Bi_3O_4Cl. *Z. Kristallogr. - New Cryst. Struct.* **1998**, *213*, 735.
(26) Eggenweiler, U.; Keller, E.; Krämer, V. Redetermination of the crystal structures of the 'Arppe compound' $Bi_{24}O_{31}Cl_{10}$ and the isomorphous $Bi_{24}O_{31}Br_{10}$. *Acta Crystallogr.* **2000**, *B56*, 431−437.
(27) Li, J.; Li, H.; Zhan, G.; Zhang, L. Solar Water Splitting and Nitrogen Fixation with Layered Bismuth Oxyhalides. *Acc. Chem. Res.* **2017**, *50*, 112−121.
(28) Jin, X.; Ye, L.; Xie, H.; Chen, G. Bismuth-rich bismuth oxyhalides for environmental and energy photocatalysis. *Coord. Chem. Rev.* **2017**, *349*, 84−101.
(29) Liao, X.; Lan, X.; Ni, N.; Yang, P.; Yang, Y.; Chen, X. Bismuth Oxychloride Nanowires for Photocatalytic Decomposition of Organic Dyes. *ACS Appl. Nano Mater.* **2021**, *4*, 3887−3892.
(30) Li, J.; Yu, Y.; Zhang, L. Bismuth Oxyhalide Nanomaterials: Layered Structures Meet Photocatalysis. *Nanoscale* **2014**, *6*, 8473−8488.
(31) Ganose, A. M.; Cuff, M.; Butler, K. T.; Walsh, A.; Scanlon, D. O. Interplay of Orbital and Relativistic Effects in Bismuth Oxyhalides: BiOF, BiOCl, BiOBr, and BiOI. *Chem. Mater.* **2016**, *28*, 1980−1984.
(32) Xiao, X.; Liu, C.; Hu, R.; Zuo, X.; Nan, J.; Li, L.; Wang, L. Oxygen-rich bismuth oxyhalides: generalized one-pot synthesis, band structures and visible-light photocatalytic properties. *J. Mater. Chem.* **2012**, *22*, 22840−22843.
(33) Di, J.; Xia, J.; Chisholm, M. F.; Zhong, J.; Chen, C.; Cao, X.; Dong, F.; Chi, Z.; Chen, H.; Weng, Y. X.; Xiong, J.; Yang, S. Z.; Li, H.; Liu, Z.; Dai, S. Defect-Tailoring Mediated Electron-Hole Separation in Single-Unit-Cell Bi_3O_4Br Nanosheets for Boosting Photocatalytic Hydrogen Evolution and Nitrogen Fixation. *Adv. Mater.* **2019**, *31*, No. 1807576.
(34) Jensen, A. A.; Hoffman, L.; Møller, B. T.; Schmidt, A.; Christiansen, K.; Elkington, J.; Dijk, F. v.*Life Cycle Assessment (LCA) - A Guide to Approaches, Experiences and Information Sources.*; European Environment Agency, 1997.
(35) Battelle; Franklin Associates Ltd.*Life-Cycle Assessment: Inventory Guidelines and Principles*; EPA/600/SR-92/245; United States Environmental Protection Agency, 1993.
(36) *ISO 14040:2006 Environmental Management — Life Cycle Assessment — Principles and Framework*; International Organization for Standardization, 2006.
(37) *ISO 14044:2006 Environmental Management — Life Cycle Assessment — Requirements and Guidelines*; International Organization for Standardization, 2006.
(38) Xu, K.; Wang, L.; Xu, X.; Dou, S. X.; Hao, W.; Du, Y. Two dimensional bismuth-based layered materials for energy-related applications. *Energy Stor. Mater.* **2019**, *19*, 446−463.
(39) Hopfgarten, F. The Crystal Structure of $Bi_{12}O_{15}Cl_{16}$. *Acta Crystallogr.* **1976**, *B32*, 2570−2573.
(40) Keller, E.; Krämer, V.; Schmidt, M.; Oppermann, H. The crystal structure of $Bi_4O_5I_2$ and its relation to the structure of $Bi_4O_5Br_2$. *Z. Kristallogr. - Cryst. Mater.* **2002**, *217*, 256−264.
(41) Mohan, R. Green bismuth. *Nat. Chem.* **2010**, *2*, 336.
(42) Naumov, A. V. World market of bismuth: A review. *Russ. J. Non-Ferr. Met.* **2007**, *48*, 10−16.
(43) Brown, T. J.; Idoine, N. E.; Wrighton, C. E.; Raycraft, E. R.; Hobbs, S. F.; Shaw, R. A.; Everett, P.; Deady, E. A.; Kresse, C.*World Mineral Production 2015−2019*; British Geological Survey: Keyworth, Nottingham, 2021. https://www2.bgs.ac.uk/mineralsuk/download/world_statistics/2010s/WMP_2015_2019.pdf (accessed 2022−10−01).
(44) *Mineral Commodity Summaries 2022*; U.S. Geological Survey: Reston, VA, 2022. https://pubs.usgs.gov/periodicals/mcs2022/mcs2022.pdf (accessed 2022−10−01).
(45) Ojebuoboh, F. K. Bismuth—Production, Properties, and Applications. *JOM* **1992**, *44*, 46−49.
(46) Nassar, N. T.; Brainard, J.; Gulley, A.; Manley, R.; Matos, G.; Lederer, G.; Bird, L. R.; Pineault, D.; Alonso, E.; Gambogi, J.; Fortier, S. M. Evaluating the mineral commodity supply risk of the U.S. manufacturing sector. *Sci. Adv.* **2020**, *6*, No. eaay8647.
(47) U.S. Department of the Interior, Office of the SecretaryFinal List of Critical Materials 2018. *Federal Registrar*: 2018; Vol. *83*, pp 23295−23296.
(48) Bobba, S.; Carrara, S.; Huisman, J.; Mathieux, F.; Pavel, C.*Critical Raw Materials for Strategic Technologies and Sectors in the EU - A Foresight Study*; European Commission, 2020.
(49) Blazy, P.; Hermant, V. Métallurgie extractive du bismuth. *Techniques de L'ingénieur: Élaboration et recyclage des métaux non ferreux* **2013**, M2316 - 1-4.
(50) Deady, E.; Moon, C.; Moore, K.; Goodenough, K. M.; Shail, R. K. Bismuth: Economic geology and value chains. *Ore Geol. Rev.* **2022**, *143*, 104722.
(51) Van den Tweel, M.*Environmental Assessment of Metals: Through Dynamic Modelling of the Metal Life Cycle System*. M.S. Thesis. Delft University of Technology, Delft, Netherlands, 2002.
(52) González-Domínguez, J. A.; Peters, E.; Dreisinger, D. B. The refining of lead by the Betts process. *J. Appl. Electrochem.* **1991**, *21*, 189−202.
(53) Davey, T. R. A. Debismuthizing of Lead. *J. Met.* **1956**, *8*, 341−350.
(54) Davey, T. R. A.The Physical Chemistry of Lead Refining. In *Lead-Zinc-Tin '80: Proceedings of a World Symposium on Metallurgy and Environmental Control*, 1980; pp 477−507.
(55) Ekman Nilsson, A.; Macias Aragonés, M.; Arroyo Torralvo, F.; Dunon, V.; Angel, H.; Komnitsas, K.; Willquist, K. A Review of the Carbon Footprint of Cu and Zn Production from Primary and Secondary Sources. *Minerals* **2017**, *7*, 168.
(56) Jones, T. D. The Harris Process of Lead Refining. *Wis. Eng.* **1929**, *33* (239), 266−268.
(57) Dupont, D.; Arnout, S.; Jones, P. T.; Binnemans, K. Antimony Recovery from End-of-Life Products and Industrial Process Residues: A Critical Review. *J. Sustain. Metall.* **2016**, *2*, 79−103.
(58) Nikolić, B. G. Processing of alkali antimony intermediate products in a lead refinery. *Hydrometallurgy* **1997**, *47*, 31−36.
(59) Li, Z.; Zhang, W.; Xia, B.; Wang, C. Comparison of Life Cycle Environmental Impact between Two Processes for Silver Separation from Copper Anode Slime. *Int. J. Environ. Res. Public Health* **2022**, *19*, 7790.
(60) Hulst, G. P. Process for Refining and Desilvering Lead. *Ind. Eng. Chem.* **1911**, *3*, 959.
(61) Frischknecht, R.; Jungbluth, N.; Althaus, H.-J.; Doka, G.; Dones, R.; Heck, T.; Hellweg, S.; Hischier, R.; Nemecek, T.; Rebitzer, G.; Spielmann, M. The ecoinvent Database: Overview and Methodological Framework. *Int. J. Life Cycle Assess.* **2005**, *10*, 3−9.
(62) Nuss, P.; Eckelman, M. J. Life cycle assessment of metals: a scientific synthesis. *PLoS One* **2014**, *9*, No. e101298.
(63) Andrae, A. S. G.; Itsubo, N.; Yamaguchi, H.; Inaba, A. Life Cycle Assessment of Japanee High-Temperature Conductive Adhesives. *Environ. Sci. Technol.* **2008**, *42*, 3084−3089.
(64) Ibn-Mohammed, T.; Reaney, I. M.; Koh, S. C. L.; Acquaye, A.; Sinclair, D. C.; Randall, C. A.; Abubakar, F. H.; Smith, L.; Schileo, G.; Ozawa-Meida, L. Life cycle assessment and environmental profile evaluation of lead-free piezoelectrics in comparison with lead zirconate titanate. *J. Eur. Ceram. Soc.* **2018**, *38*, 4922−4938.
(65) Norgate, T. E.; Jahanshahi, S.; Rankin, W. J. Assessing the environmental impact of metal production processes. *J. Cleaner Prod.* **2007**, *15*, 838−848.
(66) Wang, D.; Liu, Z.-P.; Yang, W.-M. Revealing the Size Effect of Platinum Cocatalyst for Photocatalytic Hydrogen Evolution on TiO_2 Support: A DFT Study. *ACS Catal.* **2018**, *8*, 7270−7278.
(67) Althaus, H.-J.; Hischier, R.; Osses, M.; Primas, A.; Hellweg, S.; Jungbluth, N.; Chudacoff, M.Life Cycle Inventories of Chemicals. *EcoInvent Centre*; Swiss Centre for Life Cycle Inventories, 2007.
(68) Ye, L.; Su, Y.; Jin, X.; Xie, H.; Zhang, C. Recent advances in BiOX (X = Cl, Br and I) photocatalysts: synthesis, modification, facet effects and mechanisms. *Environ. Sci.: Nano* **2014**, *1*, 90−112.

(69) Lv, X.; Lam, F. L. Y.; Hu, X. A Review on Bismuth Oxyhalide (BiOX, X = Cl, Br, I) Based Photocatalysts for Wastewater Remediation. *Front. Catal.* **2022**, *2*, 839072.
(70) Henle, J.; Simon, P.; Frenzel, A.; Scholz, S.; Kaskel, S. Nanosized BiOX (X = Cl, Br, I) Particles Synthesized in Reverse Microemulsions. *Chem. Mater.* **2007**, *19*, 366−373.
(71) Wei, X.; Akbar, M. U.; Raza, A.; Li, G. A review on bismuth oxyhalide based materials for photocatalysis. *Nanoscale Adv.* **2021**, *3*, 3353−3372.
(72) Armelao, L.; Bottaro, G.; Maccato, C.; Tondello, E. Bismuth oxychloride nanoflakes: interplay between composition-structure and optical properties. *Dalton Trans.* **2012**, *41*, 5480−5.
(73) Song, Z.; Dong, X.; Wang, N.; Zhu, L.; Luo, Z.; Fang, J.; Xiong, C. Efficient photocatalytic defluorination of perfluorooctanoic acid over BiOCl nanosheets via a hole direct oxidation mechanism. *Chem. Eng. J.* **2017**, *317*, 925−934.
(74) Jiang, J.; Zhao, K.; Xiao, X.; Zhang, L. Synthesis and facet-dependent photoreactivity of BiOCl single-crystalline nanosheets. *J. Am. Chem. Soc.* **2012**, *134*, 4473−6.
(75) Liu, W.; Shang, Y.; Zhu, A.; Tan, P.; Liu, Y.; Qiao, L.; Chu, D.; Xiong, X.; Pan, J. Enhanced performance of doped BiOCl nanoplates for photocatalysis: understanding from doping insight into improved spatial carrier separation. *J. Mater. Chem. A* **2017**, *5*, 12542−12549.
(76) Gao, X.; Peng, W.; Tang, G.; Guo, Q.; Luo, Y. Highly efficient and visible-light-driven BiOCl for photocatalytic degradation of carbamazepine. *J. Alloys Compd.* **2018**, *757*, 455−465.
(77) Ye, L.; Gong, C.; Liu, J.; Tian, L.; Peng, T.; Deng, K.; Zan, L. $Bi_n(Tu)_xCl_{3n}$: a novel sensitizer and its enhancement of BiOCl nanosheets' photocatalytic activity. *J. Mater. Chem.* **2012**, *22*, 8354−8360.
(78) Gordon, M. N.; Chatterjee, K.; Lambright, A. L.; Bueno, S. L. A.; Skrabalak, S. E. Organohalide Precursors for the Continuous Production of Photocatalytic Bismuth Oxyhalide Nanoplates. *Inorg. Chem.* **2021**, *60*, 4218−4225.
(79) Yan, X.; Zhao, H.; Li, T.; Zhang, W.; Liu, Q.; Yuan, Y.; Huang, L.; Yao, L.; Yao, J.; Su, H.; Su, Y.; Gu, J.; Zhang, D. In situ synthesis of BiOCl nanosheets on three-dimensional hierarchical structures for efficient photocatalysis under visible light. *Nanoscale* **2019**, *11*, 10203−10208.
(80) Bai, Y.; Chen, T.; Wang, P.; Wang, L.; Ye, L. Bismuth-rich $Bi_4O_5X_2$ (X = Br, and I) nanosheets with dominant {101} facets exposure for photocatalytic H_2 evolution. *Chem. Eng. J.* **2016**, *304*, 454−460.
(81) Cui, P.; Wang, J.; Wang, Z.; Chen, J.; Xing, X.; Wang, L.; Yu, R. Bismuth oxychloride hollow microspheres with high visible light photocatalytic activity. *Nano Res.* **2016**, *9*, 593−601.
(82) Ntouros, V.; Kousis, I.; Papadaki, D.; Pisello, A. L.; Assimakopoulos, M. N. Life Cycle Assessment on Different Synthetic Routes of ZIF-8 Nanomaterials. *Energies* **2021**, *14*, 4998.
(83) Sendão, R.; Yuso, M. d. V. M. d.; Algarra, M.; Esteves da Silva, J. C. G.; Pinto da Silva, L. Comparative life cycle assessment of bottom-up synthesis routes for carbon dots derived from citric acid and urea. *J. Cleaner Prod.* **2020**, *254*, 120080.
(84) Papadaki, D.; Foteinis, S.; Mhlongo, G. H.; Nkosi, S. S.; Motaung, D. E.; Ray, S. S.; Tsoutsos, T.; Kiriakidis, G. Life cycle assessment of facile microwave-assisted zinc oxide (ZnO) nanostructures. *Sci. Total Environ.* **2017**, *586*, 566−575.
(85) Wu, F.; Zhou, Z.; Hicks, A. L. Life Cycle Impact of Titanium Dioxide Nanoparticle Synthesis through Physical, Chemical, and Biological Routes. *Environ. Sci. Technol.* **2019**, *53*, 4078−4087.
(86) Li, Y.; Jiang, H.; Wang, X.; Hong, X.; Liang, B. Recent advances in bismuth oxyhalide photocatalysts for degradation of organic pollutants in wastewater. *RSC Adv.* **2021**, *11*, 26855−26875.
(87) Ye, L.; Jin, X.; Leng, Y.; Su, Y.; Xie, H.; Liu, C. Synthesis of black ultrathin BiOCl nanosheets for efficient photocatalytic H2 production under visible light irradiation. *J. Power Sources* **2015**, *293*, 409−415.
(88) Zhang, K.; Liu, C.; Huang, F.; Zheng, C.; Wang, W. Study of the electronic structure and photocatalytic activity of the BiOCl photocatalyst. *Appl. Catal., B* **2006**, *68*, 125−129.
(89) Cheng, H.; Huang, B.; Dai, Y. Engineering BiOX (X = Cl, Br, I) nanostructures for highly efficient photocatalytic applications. *Nanoscale* **2014**, *6*, 2009−26.
(90) Zhang, L.; Han, Z.; Wang, W.; Li, X.; Su, Y.; Jiang, D.; Lei, X.; Sun, S. Solar-Light-Driven Pure Water Splitting with Ultrathin BiOCl Nanosheets. *Chem.—Eur. J.* **2015**, *21*, 18089−18094.
(91) Wenderich, K.; Mul, G. Methods, Mechanism, and Applications of Photodeposition in Photocatalysis: A Review. *Chem. Rev.* **2016**, *116*, 14587−14619.
(92) Ni, M.; Leung, M. K. H.; Leung, D. Y. C.; Sumathy, K. A review and recent developments in photocatalytic water-splitting using TiO_2 for hydrogen production. *Renewable Sustainable Energy Rev.* **2007**, *11*, 401−425.
(93) Nørskov, J. K.; Bligaard, T.; Logadottir, A.; Kitchin, J. R.; Chen, J. G.; Pandelov, S.; Stimming, U. Trends in the Exchange Current for Hydrogen Evolution. *J. Electrochem. Soc.* **2005**, *152*, J23−J26.
(94) You, Y.; Wang, S.; Xiao, K.; Ma, T.; Zhang, Y.; Huang, H. Z-Scheme g-C_3N_4/Bi_4NbO_8Cl Heterojunction for Enhanced Photocatalytic Hydrogen Production. *ACS Sustainable Chem. Eng.* **2018**, *6*, 16219−16227.
(95) Ozaki, D.; Suzuki, H.; Tomita, O.; Inaguma, Y.; Nakashima, K.; Kageyama, H.; Abe, R. A new lead-free Sillén-Aurivillius oxychloride $Bi_5SrTi_3O_{14}Cl$ with triple-perovskite layers for photocatalytic water splitting under visible light. *J. Photochem. Photobiol., A* **2021**, *408*, 113095.
(96) Dong, X. D.; Zhang, Y. M.; Zhao, Z. Y. Role of the Polar Electric Field in Bismuth Oxyhalides for Photocatalytic Water Splitting. *Inorg. Chem.* **2021**, *60*, 8461−8474.
(97) Yang, J.; Wang, D.; Han, H.; Li, C. Roles of Cocatalysts in Photocatalysis and Photoelectrocatalysis. *Acc. Chem. Res.* **2013**, *46*, 1900−1909.
(98) Xu, L.; Chen, W.-q.; Ke, S.-q.; Zhang, S.-m.; Zhu, M.; Zhang, Y.; Shi, W.-y.; Horike, S.; Tang, L. Construction of heterojunction Bi/Bi_5O_7I/Sn_3O_4 for efficient noble-metal-free Z-scheme photocatalytic H_2 evolution. *Chem. Eng. J.* **2020**, *382*, 122810.
(99) Shang, J.; Hao, W.; Lv, X.; Wang, T.; Wang, X.; Du, Y.; Dou, S.; Xie, T.; Wang, D.; Wang, J. Bismuth Oxybromide with Reasonable Photocatalytic Reduction Activity under Visible Light. *ACS Catal.* **2014**, *4*, 954−961.
(100) Umezawa, N.; Shuxin, O.; Ye, J. Theoretical study of high photocatalytic performance of Ag3PO4. *Phys. Rev. B* **2011**, *83* (3), 035202.
(101) Wang, Y.; Meng, J.; Jing, S.; Wang, K.; Ban, C.; Feng, Y.; Duan, Y.; Ma, J.; Gan, L.; Zhou, X. Origin of Bismuth-Rich Strategy in Bismuth Oxyhalide Photocatalysts. *Energy Environ. Mater.* **2022**, No. e12432.
(102) Mi, Y.; Wen, L.; Wang, Z.; Cao, D.; Xu, R.; Fang, Y.; Zhou, Y.; Lei, Y. Fe(III) modified BiOCl ultrathin nanosheet towards high-efficient visible-light photocatalyst. *Nano Energy* **2016**, *30*, 109−117.
(103) Capello, C.; Fischer, U.; Hungerbühler, K. What is a green solvent? A comprehensive framework for the environmental assessment of solvents. *Green Chem.* **2007**, *9*, 927−934.
(104) Fernandes, S.; Esteves da Silva, J. C. G.; Pinto da Silva, L. Life Cycle Assessment of the Sustainability of Enhancing the Photodegradation Activity of TiO_2 with Metal-Doping. *Materials* **2020**, *13*, 1487.
(105) Wang, J.; Liao, T.; Wei, Z.; Sun, J.; Guo, J.; Sun, Z. Heteroatom-Doping of Non-Noble Metal-Based Catalysts for Electrocatalytic Hydrogen Evolution: An Electronic Structure Tuning Strategy. *Small Methods* **2021**, *5*, No. 2000988.
(106) Huang, F.; Yan, A.; Zhao, H., Influences of Doping on Photocatalytic Properties of TiO_2 Photocatalyst. In *Semiconductor Photocatalysis-Materials, Mechanisms and Applications*; InTech, 2016; pp 31−80.
(107) Xiao, H.; Liu, P.; Wang, W.; Ran, R.; Zhou, W.; Shao, Z. Enhancing the photocatalytic activity of Ruddlesden-Popper Sr_2TiO_4 for hydrogen evolution through synergistic silver doping and moderate reducing pretreatment. *Mater. Today Energy* **2022**, *23*, 100899.

https://doi.org/10.1021/acssuschemeng.2c05326
ACS Sustainable Chem. Eng. 2022, 10, 15622−15641

(108) Hsieh, P. A.; Chen, P. J.; Lyu, L. M.; Chen, S. Y.; Tseng, M. C.; Chung, M. Y.; Chiang, W. H.; Chen, J. L.; Kuo, C. H. Enhanced Production of Formic Acid in Electrochemical CO_2 Reduction over Pd-Doped BiOCl Nanosheets. *ACS Appl. Mater. Interfaces* **2021**, *13*, 58799−58808.
(109) Wang, S.; Meng, C.; Bai, Y.; Wang, Y.; Liu, P.; Pan, L.; Zhang, L.; Yin, Z.; Tang, N. Synergy Promotion of Elemental Doping and Oxygen Vacancies in Fe_2O_3 Nanorods for Photoelectrochemical Water Splitting. *ACS Appl. Nano Mater.* **2022**, *5*, 6781−6791.
(110) Li, J.; Zhao, K.; Yu, Y.; Zhang, L. Facet-Level Mechanistic Insights into General Homogeneous Carbon Doping for Enhanced Solar-to-Hydrogen Conversion. *Adv. Funct. Mater.* **2015**, *25*, 2189−2201.
(111) Wei, Z.; Liu, J.; Fang, W.; Qin, Z.; Jiang, Z.; Shangguan, W. A visible-light driven novel layered perovskite oxyhalide Bi_4MO_8X (M = Nb, Ta; X = Cl, Br) constructed using BiOX (X = Cl, Br) for enhanced photocatalytic hydrogen evolution. *Catal. Sci. Technol.* **2018**, *8*, 3774−3784.
(112) Fujito, H.; Kunioku, H.; Kato, D.; Suzuki, H.; Higashi, M.; Kageyama, H.; Abe, R. Layered Perovskite Oxychloride Bi_4NbO_8Cl: A Stable Visible Light Responsive Photocatalyst for Water Splitting. *J. Am. Chem. Soc.* **2016**, *138*, 2082−2085.
(113) Tao, X.; Zhao, Y.; Mu, L.; Wang, S.; Li, R.; Li, C. Bismuth Tantalum Oxyhalogen: A Promising Candidate Photocatalyst for Solar Water Splitting. *Adv. Energy Mater.* **2018**, *8*, 1701392.
(114) Chatterjee, K.; Dos Reis, R.; Harada, J. K.; Mathiesen, J. K.; Bueno, S. L. A.; Jensen, K. M. Ø.; Rondinelli, J. M.; Dravid, V.; Skrabalak, S. E. Durable Multimetal Oxychloride Intergrowths for Visible Light-Driven Water Splitting. *Chem. Mater.* **2021**, *33*, 347−358.
(115) Chatterjee, K.; Bueno, S.; Skrabalak, S.; Dravid, V.; Reis, R. d. Nanoscale Investigation of Layered Oxychloride Intergrowth Photocatalysts for Visible Light Driven Water Splitting. *Microsc. Microanal.* **2020**, *26*, 376−379.
(116) Kato, D.; Hongo, K.; Maezono, R.; Higashi, M.; Kunioku, H.; Yabuuchi, M.; Suzuki, H.; Okajima, H.; Zhong, C.; Nakano, K.; Abe, R.; Kageyama, H. Valence Band Engineering of Layered Bismuth Oxyhalides toward Stable Visible-Light Water Splitting: Madelung Site Potential Analysis. *J. Am. Chem. Soc.* **2017**, *139*, 18725−18731.
(117) Walsh, A.; Payne, D. J.; Egdell, R. G.; Watson, G. W. Stereochemistry of post-transition metal oxides: revision of the classical lone pair model. *Chem. Soc. Rev.* **2011**, *40*, 4455−4463.
(118) Sultana, S.; Mansingh, S.; Parida, K. M. Crystal facet and surface defect engineered low dimensional CeO_2 (0D, 1D, 2D) based photocatalytic materials towards energy generation and pollution abatement. *Mater. Adv.* **2021**, *2*, 6942−6983.
(119) Zhao, K.; Zhang, L.; Wang, J.; Li, Q.; He, W.; Yin, J. J. Surface structure-dependent molecular oxygen activation of BiOCl single-crystalline nanosheets. *J. Am. Chem. Soc.* **2013**, *135* (42), 15750−15753.
(120) Lee, G.-J.; Zheng, Y.-C.; Wu, J. J. Fabrication of hierarchical bismuth oxyhalides (BiOX, X = Cl, Br, I) materials and application of photocatalytic hydrogen production from water splitting. *Catal. Today* **2018**, *307*, 197−204.
(121) Komarneni, S.; Noh, Y. D.; Kim, J. Y.; Kim, S. H.; Katsuki, H. Solvothermal/Hydrothermal Synthesis of Metal Oxides and Metal Powders with and without Microwaves. *Z. Naturforsch., B: J. Chem. Sci.* **2010**, *65*, 1033−1037.
(122) Pan, H.; Feng, L.; Liu, P.; Zheng, X.; Zhang, X. Asymmetric surfaces endow Janus bismuth oxyhalides with enhanced electronic and catalytic properties for the hydrogen evolution reaction. *J. Colloid Interface Sci.* **2022**, *617*, 204−213.
(123) Li, J.; Zhan, G.; Yu, Y.; Zhang, L. Superior visible light hydrogen evolution of Janus bilayer junctions via atomic-level charge flow steering. *Nat. Commun.* **2016**, *7*, 11480.
(124) Li, Y.; Zhang, J.; Chen, Q.; Xia, X.; Chen, M. Emerging of Heterostructure Materials in Energy Storage: A Review. *Adv. Mater.* **2021**, *33*, No. 2100855.
(125) Liu, Y.; Lv, P.; Zhou, W.; Hong, J. Built-In Electric Field Hindering Photogenerated Carrier Recombination in Polar Bilayer SnO/BiOX (X = Cl, Br, I) for Water Splitting. *J. Phys. Chem. C* **2020**, *124*, 9696−9702.
(126) Kandi, D.; Martha, S.; Thirumurugan, A.; Parida, K. M. Modification of BiOI Microplates with CdS QDs for Enhancing Stability, Optical Property, Electronic Behavior toward Rhodamine B Decolorization, and Photocatalytic Hydrogen Evolution. *J. Phys. Chem. C* **2017**, *121*, 4834−4849.
(127) Gan, H.-F.; Meng, X.-S.; Song, C.-H.; Li, B.-X. A Survey on Health Effects in a Human Population Exposed to Permanent-Waving Solution Containing Thioglycolic Acid. *J. Occup. Health* **2003**, *45*, 400−404.
(128) Abdelhamid, H. N.; Wu, H. F. Probing the interactions of chitosan capped CdS quantum dots with pathogenic bacteria and their biosensing application. *J. Mater. Chem. B* **2013**, *1*, 6094−6106.
(129) Zhang, Y.; Zhou, W.; Jia, L.; Tan, X.; Chen, Y.; Huang, Q.; Shao, B.; Yu, T. Visible light driven hydrogen evolution using external and confined CdS: Effect of chitosan on carriers separation. *Appl. Catal., B* **2020**, *277*, 119152.
(130) Guinée, J. B.; Heijungs, R.; Huppes, G.; Zamagni, A.; Masoni, P.; Buonamici, R.; Ekvall, T.; Rydberg, T. Life Cycle Assessment: Past, Present, and Future. *Environ. Sci. Technol.* **2011**, *45*, 90−96.
(131) *Critical Raw Materials Resilience: Charting a Path towards greater Security and Sustainability*; Communication from the Commission to the European Parliament; the Council, European Economic and Social Committee and the Committee of the Regions, 2020.
(132) Gislev, M.; Grohol, M.*Report on Critical Raw Materials and the Circular Economy*; European Commission, 2018.
(133) Corsi, S. R.; Graczyk, D. J.; Geis, S. W.; Booth, N. L.; Richards, K. D. A Fresh Look at Road Salt: Aquatic Toxicity and Water-Quality Impacts on Local, Regional, and National Scales. *Environ. Sci. Technol.* **2010**, *44*, 7376−7382.
(134) Peplow, M.Solar Panels Face Recycling Challenge. *Chem. Eng. News*; May 23, 2022; pp 24−28.
(135) Peplow, M. Solar Panels Face Recycling Challenge. *ACS Cent. Sci.* **2022**, *8*, 299−302.
(136) Walzberg, J.; Carpenter, A.; Heath, G. A. Role of the social factors in success of solar photovoltaic reuse and recycle programmes. *Nat. Energy* **2021**, *6*, 913−924.
(137) Tao, M.; Fthenakis, V.; Ebin, B.; Steenari, B. M.; Butler, E.; Sinha, P.; Corkish, R.; Wambach, K.; Simon, E. S. Major challenges and opportunities in silicon solar module recycling. *Prog. Photovolt Res. Appl.* **2020**, *28*, 1077−1088.
(138) Wu, J.; Zhang, Q.; Xu, Z. Research on China's photovoltaic modules recycling models under extended producer responsibility. *Int. J. Sustain. Eng.* **2019**, *12*, 423−432.
(139) Heath, G. A.; Silverman, T. J.; Kempe, M.; Deceglie, M.; Ravikumar, D.; Remo, T.; Cui, H.; Sinha, P.; Libby, C.; Shaw, S.; Komoto, K.; Wambach, K.; Butler, E.; Barnes, T.; Wade, A. Research and development priorities for silicon photovoltaic module recycling to support a circular economy. *Nat. Energy* **2020**, *5*, 502−510.
(140) Lunardi, M.; Alvarez-Gaitan, J.; Bilbao, J.; Corkish, R. Comparative Life Cycle Assessment of End-of-Life Silicon Solar Photovoltaic Modules. *Appl. Sci.* **2018**, *8*, 1396.
(141) Latunussa, C. E. L.; Ardente, F.; Blengini, G. A.; Mancini, L. Life Cycle Assessment of an innovative recycling process for crystalline silicon photovoltaic panels. *Sol. Energy Mater. Sol. Cells* **2016**, *156*, 101−111.
(142) Photovoltaic module stewardship and takeback program−Definitions−Requirements−Enforcement−Fees−Rule making. In *Revised Code of Washington*, Chapter 70A.510.010, 2021.
(143) Deng, R.; Dias, P. R.; Lunardi, M. M.; Ji, J. A sustainable chemical process to recycle end-of-life silicon solar cells. *Green Chem.* **2021**, *23*, 10157−10167.

https://doi.org/10.1021/acssuschemeng.2c05326
ACS Sustainable Chem. Eng. 2022, 10, 15622−15641